4

Physiology of the Vestibular Organs

The vestibular organs monitor the motion of the head and the forces acting on it. As we have already noted in earlier chapters, each semicircular canal measures the angular motion of the head around a single axis, while the three canals, given their nearly orthogonal orientation, provide the brain with a three-dimensional reconstruction of this motion. Similarly, the two otolith organs furnish a three-dimensional reconstruction of translational motion. In addition, the otolith organs, because of their sensitivity to linear forces, respond to tilts that change the orientation of the head with respect to the earth's gravitational field.

Given the differences in their design and function, we will consider the canals and otolith organs separately. Before doing so, however, we summarize features that are common to both sets of organs. The chapter emphasizes two approaches that are of particular importance in understanding the function of an organ: 1) its biomechanics, which determines how motion of the head is coupled to hair-bundle deflection; and 2) afferent discharge, which is the result of the several stages of transduction, and describes the information delivered by the vestibular nerve to the brain. Consistent with the overall emphasis of this book, we concentrate on mammals. Studies in other vertebrates have been summarized elsewhere (Lysakowski and Goldberg 2004).

4.1 GENERAL FEATURES OF THE VESTIBULAR ORGANS

Vestibular Organs are Inertial Sensors

A critical event in transduction is the bending of hair bundles as a result of the displacement of a gelatinous accessory structure, either the cupula or otoconial membrane, relative to the apical surface of the neuroepithelium. Displacement takes place on three space scales. *Macromechanics* refers to the bulk movement of the accessory structure, together with the associated movement of other labyrinthine structures and fluids. The coupling of hair bundles to the accessory structure is referred to as *micromechanics*, while the linkage between bundle displacement and transducer channel opening may be termed *nanomechanics*. For now we concentrate on macromechanics.

Both the semicircular canals and the otoconial or otolith organs can be considered inertial sensors. Head movements are faithfully transmitted to the membranous labyrinth because it is tethered to the skull. In the case of the semicircular canals, the relative displacement of the cupula depends on the inertia of endolymph, whose rotational motion lags behind that of the membranous canal duct. As a result, the displacement of the endolymph relative to the canal wall is in a direction opposite that of the provoking

head movement. Because of fluid continuity, the cupula also moves backward with a volume displacement equal to that of the endolymph. For the otolith organs, the inertial sensors are the otoconia, calcium carbonate crystals that give the upper layer of the otoconial membrane a density greater than that of the surrounding endolymph. As a consequence of the differential density, a linear head acceleration in one direction leads to an oppositely directed shearing displacement of the otoconial membrane relative to the skull.

In Chapter 15, we make a distinction between coordinate systems and reference frames. A coordinate system is a three-dimensional vector space in which a variable is measured. In the case of the vestibular organs, the appropriate variable is head acceleration, which can be represented as a vector in inertial space. At the same time, we can choose a reference frame in which the response to a particular motion is invariant. For the labyrinth, response is determined by the orientation of head motion relative to head-fixed receptors. For example, a semicircular canal will respond in the same way to a leftward head rotation whether the subject is upright or upside down even though the vector representing motion rotates by 180 degrees when expressed in earth-fixed coordinates. The motion vector, when transformed from earth-fixed to head-fixed coordinates, remains constant, as does the response. For the labyrinth, then, it is best to express motion vectors in a head-fixed reference frame. Yet as we shall see in Chapter 15, the brain can combine information from otolith organs and semicircular canals to transform the reference frame from being head-fixed to being earth-fixed.

Resting Discharge

As first described by Lowenstein and Sand (1936), canal afferents continue to discharge even in the absence of head rotations. A resting discharge offers several advantages. First, as illustrated in Figure 4.1, it allows each fiber to respond bidirectionally, increasing its discharge when the head moves in one direction and decreasing it for head motion in the opposite direction. A discharge increase is referred to as an *excitation* and a decrease as an *inhibition*. This is so even though the decrease might

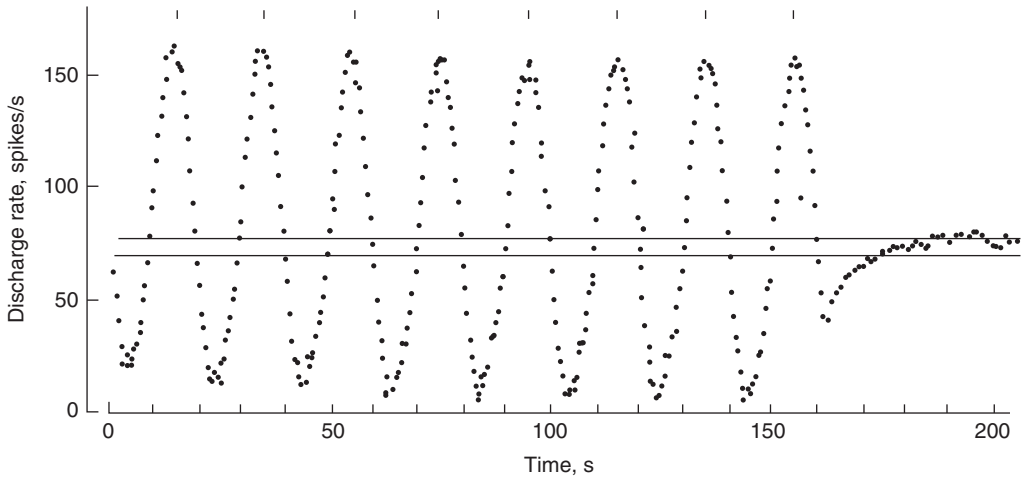

Figure 4.1 Bidirectional response of a vestibular-nerve afferent to sinusoidal head rotations, 0.05 Hz, 80 deg/s. In its response, the discharge of this anterior canal afferent increases during cupular deflections towards the canal duct and decreases during oppositely directed deflections. In passing from excitation to inhibition, there is no discontinuity, such as would occur were there a sensory threshold. *Vertical marks* indicate instants of peak excitatory velocity. *Lower* and *upper horizontal lines*, respectively, indicate resting discharge before and after stimulation. (From Fernández and Goldberg 1971)

properly be called a *disfacilitation* since it is based on a decrease in transducer current, which in turn results in a decreased release of excitatory neurotransmitter from hair cells (see Chapter 3). Second, resting activity can reduce, if not eliminate, the existence of a sensory threshold. As discharge in Figure 4.1 passes through its resting value, there is no sign of a discontinuity. Third, resting activity provides a powerful excitatory input to the brain, as is exemplified by the drastic reduction in the resting discharge of secondary neurons in the vestibular nuclei after labyrinthectomy or vestibular-nerve section (see Chapters 13 and 16).

The resting discharge is measured in the absence of stimulation. Because semicircular-canal afferents respond to angular accelerations, their resting discharge can be determined by keeping the head stationary or having it move at a constant angular velocity. Otolith afferents respond to linear forces, including gravity. With the continual presence of gravity, an absence of stimulation is not possible terrestrially. But here use can be made of the fact that the directional properties of each otolith afferent can be characterized by a polarization vector that summarizes the response when the head is tilted in various directions with respect to the earth vertical (Angelaki and Dickman 2000; Fernández et al. 1972; Loe et al. 1973). The resting (zero-force) discharge is obtained when the polarization and gravity vectors are orthogonal. This will occur at two points during a sequence of tilts around pitch, roll or any other great circle (see Section 4.3, Directional properties, for details).

Resting discharge depends on species, organ, and discharge regularity. As will be amplified in the next section, afferents can have a regular or an irregular spacing of action potentials (Fig. 4.2). Background rates among regularly discharging canal afferents average 50 to 100 spikes/s, being higher in monkeys (Goldberg and Fernandez 1971a; Lysakowski et al. 1995) than in cats (Anderson et al. 1978; Estes et al. 1975; Tomko et al. 1981b) or various rodents (Baird et al. 1988; Curthoys 1982; Hullar and Minor 1999; Hullar et al. 2005; Schneider and Anderson, 1976). Resting rates are lower in afferents innervating otolith organs (Fernández et al. 1972; Fernández and Goldberg 1976a; Goldberg et al. 1990a) and in irregularly discharging, as compared to regularly discharging, canal afferents (Estes et al. 1975; Fernández and Goldberg 1976a; Goldberg and Fernandez 1971b; Lysakowski et al. 1995; Tomko et al. 1981b). A smaller difference is observed between regular and irregular otolith afferents (Estes et al. 1975; Goldberg and Fernandez 1971b; Goldberg et al. 1990a; Tomko et al. 1981a).

The above results were obtained in barbiturate-anesthetized preparations. Similar observations have been made in unanesthetized, decerebrate preparations (Blanks and Precht 1978; Perachio and Correia 1983; Plotnik et al. 2005) and in alert monkeys (Haque et al. 2004; Keller 1976; Lisberger and Pavelko 1986; Louie and Kimm 1976; Ramachandran and Lisberger 2006; Sadeghi et al. 2007b). In fact, except for a modest reduction in resting discharge confined to irregular afferents (Perachio and Correia 1983; Plotnik et al. 2005), anesthesia is found to have little or no effect on afferent discharge properties in mammals, although it may result in a large depression of the resting discharge in pigeons (Anastasio et al. 1985). The modest resting discharge reduction in mammals or the larger effect in pigeons may reflect a direct action of anesthesia on the labyrinth combined with an indirect action mediated by the efferent vestibular system (see Chapter 5).

Discharge Regularity

Some fibers have a regular spacing of action potentials, while in other units the spacing is irregular (Fig. 4.2). Discharge regularity has proved useful in classifying units (Goldberg 2000) There are three reasons. First, discharge regularity is characteristic of each unit. This can be seen in Figure 4.3, which plots the relation between the standard deviation of intervals (sd) and the mean interval ($\bar{t}$) for three otolith afferents whose discharge was allowed to reach a steady state at different tilt angles. The points for each unit, whether obtained during excitation, rest, or inhibition, form a single relation. Furthermore, the relations for different units do not intersect. Second, it is easy to quantify this discharge property by calculating the coefficient of variation (cv), the ratio of sd to $\bar{t}$. The cv varies with $\bar{t}$. To account for this variation, we use a normalized statistic (cv*), the cv at a standard

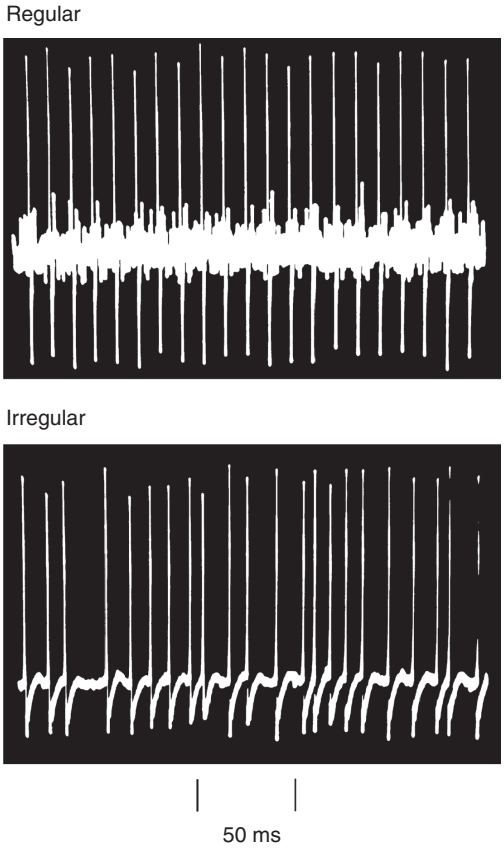

Figure 4.2 Discharge regularity in vestibular-nerve afferents. Spike trains are shown during the resting discharge for two afferents, each innervating the anterior semicircular canal in a squirrel monkey. Although both afferents have similar discharge rates, just under 100 spikes/s, they differ in the spacing of their action potentials, which is regular in the top afferent and irregular in the bottom afferent. (From Goldberg and Fernández 1971b)

mean interval. Given typical discharge rates in mammals, 15 ms provides a suitable standard interval (Fig. 4.3, vertical line). The cv* gives an unambiguous measure of discharge regularity, independent of discharge rate. Third, and most importantly, fibers classified as regularly or irregularly discharging differ in several other respects as well.

Table 4.1 summarizes some of these differences for afferents, including those innervating the cristae and the maculae. Of the several differences listed in the table, which are causally related to discharge regularity? Based on the response to externally applied galvanic currents, it was suggested that discharge regularity and encoder sensitivity are mechanistically linked (Baird et al. 1988; Ezure et al. 1983; Goldberg et al. 1984) . Galvanic responses are much larger in irregular (Fig. 4.4A) than in regular units (Fig. 4.4B). There is evidence that the currents work on afferent terminals, rather than on hair cells or parent axons (Goldberg et al. 1984). When galvanic sensitivity is plotted against cv*, a strong, almost linear relation is obtained (Fig. 4.4C). cv* varies in the population more than 20-fold, from less than 0.025 to more than 0.5, and there is a comparable variation in galvanic sensitivity.

A stochastic model of repetitive discharge can be used to explain the relation between discharge regularity and galvanic sensitivity (Smith and Goldberg 1986) (Fig. 4.5). Consistent with the treatment in Chapter 3, repetitive activity in the model reflects the interaction of an afterhyperpolarization (AHP) following each spike with synaptic and other depolarizing currents. The random timing of synaptic quanta results in synaptic noise that is responsible for the variability of interspike intervals. Consider the simulated train of a regularly discharging afferent (Fig. 4.5A). Here, each AHP is deep and slow. Synaptic currents are sufficiently intense so that the mean voltage trajectory crosses the critical firing level (CFL). Firing is said to be deterministic. The result is a regular discharge. To simulate an irregular discharge (Fig. 4.5B), the AHP is made shallower and faster. Of lesser importance, there is also an increase in the size of synaptic quanta. To reach the same discharge rate as shown for the regular unit requires much less synaptic current and the mean trajectory does not cross the CFL. Firing is non-deterministic, occurring because of the occurrence of synaptic quanta (mEPSPs). As a result, discharge reflects the random timing of the quanta and is irregular. To see why the two units also differ in their sensitivities to depolarizing inputs, we can add an externally applied depolarizing current. In the regular unit, the current shifts the mean voltage trajectory slightly upward (Fig. 4.5A, thin curve) and results in a small increase in firing rate (Fig. 4.5C). In the irregular unit, a similar upward shift results in several previously ineffective peaks in synaptic noise (Fig. 4.5B, dots) now exceeding the CFL (Fig. 4.5D) and in an increase

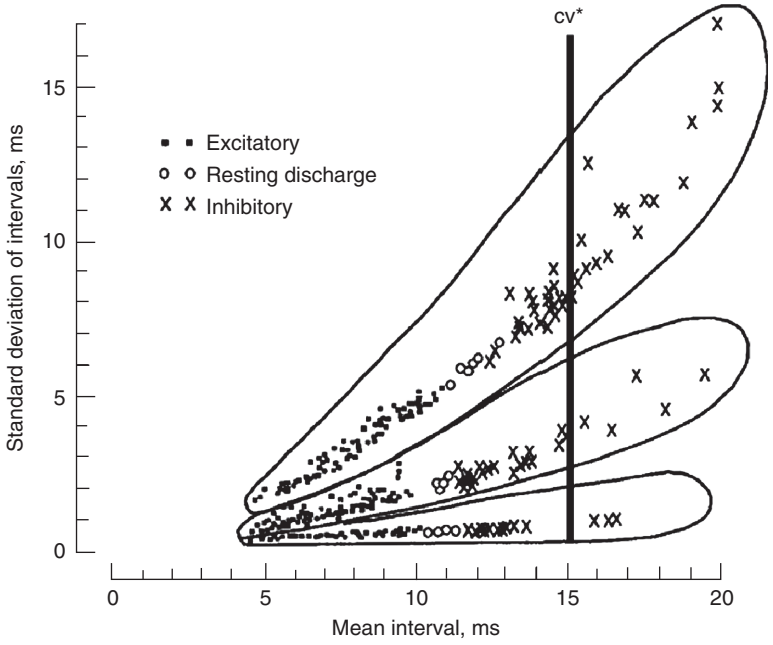

Figure 4.3 Quantifying discharge regularity. Relations between the standard deviation of intervals and the mean interval for three otolith units differing in discharge regularity. The points for each unit fall along a single trajectory and those for different units do not intersect. Data were obtained during excitation, rest, and inhibition (see Key). To characterize discharge regularity, the coefficient of variation (cv*) is calculated at a mean interval of 15 ms (*vertical line*). For the three units, cv* = 0.67 (*top*), 0.20 (*middle*), and 0.033 (*bottom*). (From Goldberg and Fernández 1971b)

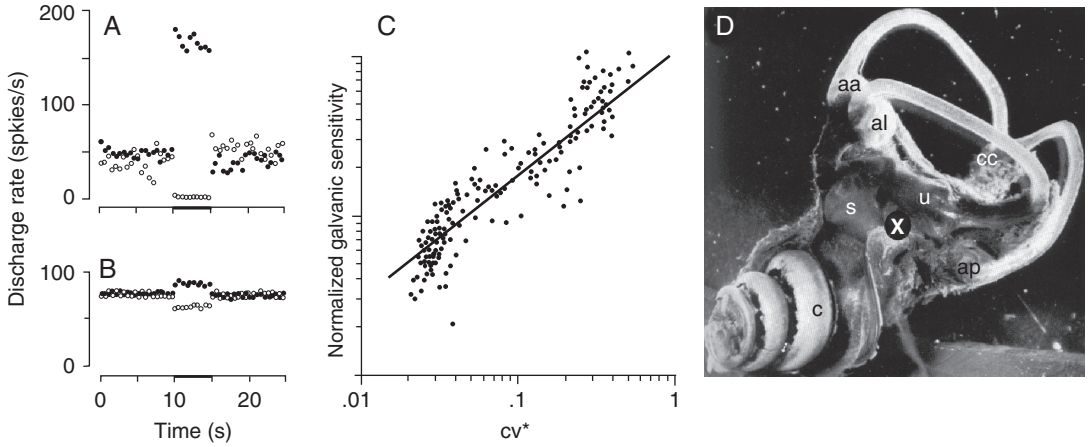

Figure 4.4 Encoder sensitivity is higher, the more irregular is the discharge of a unit. Such sensitivity is measured by galvanic currents delivered by way of the perilymphatic space. Responses of an irregularly (**A**) and a regularly discharging unit (**B**) from the same animal. Currents are delivered between 10 and 15 s (*bars*) and are of the same magnitude for both units. Cathodal currents excite (Ĉ); anodal currents inhibit (Ĉ). Responses are much larger in the irregular unit. **C**. Galvanic sensitivity versus discharge regularity (cv*) for several units. There is a strong positive relation between the two variables. **D**. In these experiments, one stimulating electrode is placed in the vestibule (*white cross*); the other (not shown) is in the middle ear. Abbreviations: *aa*, *al*, and *ap*, ampullae for the anterior, lateral, and posterior canals; *c*, cochlea; *cc*, crus commune; *s* and *u*, sacculus and utriculus. (**A–C**, from Baird et al. 1988; **D** modified from Lindeman 1969)

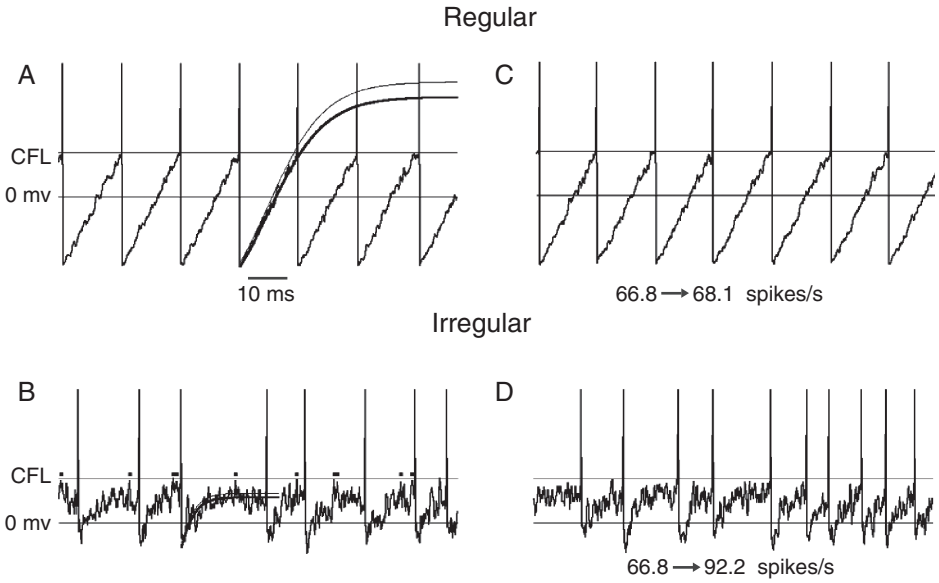

Figure 4.5 A stochastic model of repetitive discharge simulates the discharge of a regular unit (**A**) and an irregular unit (**B**). The two units differ in their afterhyperpolarizations (AHPs), which are deeper and slower in the regular unit. Resting potential, 0 mV; constant threshold for spike discharge. The random timing of quanta (mEPSPs) introduces synaptic noise in both cases. Quantal size and synaptic noise are larger in the irregular unit. Mean voltage trajectory (*thick curve*) and the effects of a galvanic current (*thin curve*) are shown for both units. The mean trajectory crosses threshold in the regular unit but not in the irregular unit. The effects of a 1-mV depolarization are shown in **C** and **D** for the two units. Sensitivity to the depolarization, measured by the increase in discharge rate, is almost 20-fold larger for the irregular unit, 25.4 vs. 1.3 spikes/s (see numbers under voltage traces). Dots in **B** mark peaks that are within 1 mV of threshold . (Based on Smith and Goldberg 1986)

in firing rate almost 20 times greater than that seen in the regular unit.

The more irregular the discharge of a unit, the greater is its sensitivity to synaptic or external currents. Given this conclusion we can interpret the entries in Table 4.1. Based on their greater encoder sensitivity, irregular fibers would be expected to have larger responses to sensory inputs, to efferent activation, and to externally applied galvanic currents. Fiber size, while it is known to affect electrical excitability (Rushton 1951), has a much smaller effect on the galvanic sensitivity of vestibular-nerve afferents than does discharge regularity (Goldberg et al. 1984; Lysakowski et al. 1995). The only difference listed in the table that is not causally related to discharge regularity involves response dynamics. Confirmation of the latter conclusion was obtained from a comparison of the response dynamics obtained with sinusoidal galvanic currents and sinusoidal head rotations (Ezure et al. 1983; Goldberg et al. 1982). In addition, the conclusion illustrates that two discharge properties—in this case discharge regularity and response dynamics—can be highly correlated without being causally related.

As indicated in Table 4.1, the response dynamics of regular and irregular afferents differ. Regular afferents have tonic response dynamics, similar to those expected of macromechanics. Irregular afferents are more phasic, implying that they are sensitive to the velocity of cupular or otolithic displacement, as well as to the displacement itself. We will return to the etiology of response dynamics later (4.2 Semicircular canals, Afferent response dynamics).

Table 4.1 Characteristics of regularly and irregularly discharging afferents, mammalian vestibular nerve

Irregularly Discharging	Regularly Discharging
Thick and medium-sized axons ending as calyx and dimorphic terminals in the central (striolar) zone.[1]	Medium-sized and thin axons ending as dimorphic and bouton terminals in the peripheral (peripheral extrastriolar) zone.
Phasic-tonic response dynamics, including a sensitivity to the velocity of cupular (otolith) displacement.[2]	Tonic response dynamics, resembling those expected of end-organ macromechanics.
High sensitivity to angular or linear forces. (Calyx units innervating the cristae have an irregular discharge and low sensitivities.)[2]	Low sensitivity to angular or linear forces.
Large responses to electrical stimulation of efferent fibers.[3]	Small responses to electrical stimulation of efferent fibers.
Low thresholds to short shocks and large responses to constant galvanic currents, both delivered via the perilymphatic space.[4]	High thresholds and small responses to the same galvanic stimuli.

[1]Goldberg and Fernandez, 1977; Yagi et al., 1977; Baird et al., 1988; Goldberg et al., 1990b; Lysakowski et al., 1995
[2]Goldberg and Fernandez, 1971b; Schneider and Anderson, 1976; Fernandez and Goldberg, 1976c; Curthoys, 1982)}(Baird et al., 1988; Goldberg et al., 1990a; Lysakowski et al., 1995
[3]Goldberg and Fernandez, 1980; McCue and Guinan, 1994; Marlinski et al., 2004
[4]Ezure et al., 1983; Goldberg et al., 1984; Bronte-Stewart and Lisberger, 1994

Information Transmission

Information theory was devised by Shannon (Shannon and Weaver 1949) to describe the uncertainty or entropy contained in an ensemble of messages (e.g., a set of stimuli or of responses). The mutual information (MI) encoded by a sensory system is defined as the average reduction in the uncertainty of the stimulus ensemble resulting from the presence of a particular response (Borst and Theunissen 1999; Rieke et al. 1997). Of particular interest in the present context is the question as to how efficiently regular and irregular spike trains encode features of the stimulus. For continuous ensembles, MI is related to the signal-to-noise ratio characterizing the stimulus or response. Interspike-interval variability during identical stimulus conditions may be viewed as noise. From this, it might be expected that irregular units would not be as efficient in stimulus encoding. This conclusion can be illustrated by a linear-systems analysis that deduces the optimal filter that, when convolved with the spike train, provides a reconstructed stimulus with minimal error from the actual stimulus (Borst and Theunissen 1999; Rieke et al. 1997). Figure 4.6 compares a regular and an irregular unit (Sadeghi et al. 2007a). The regular unit is much better at estimating the actual stimulus. Corollaries of this result are that the regular unit is better at transmitting information about the stimulus and at detecting small changes in head motion.

In Figure 4.6, the two units had similar gains. There are irregular units with considerably higher gains, which should serve to enhance their information transmission. In fact, when differences in discharge regularity are taken into account, regular and irregular units have similar MIs (Hirsch et al. 2011). One might conclude that an irregular discharge offers no functional advantage. Here, we can make two comments. First, information theory deals with the ideal handling of information transmission, not the actual way this occurs. Second, the calculation emphasizes signals (gains) and noise (discharge irregularity). Regular and irregular units differ in several other respects. It would seem safe to assume that irregular units play distinctive roles in the processing of vestibular sensation. To deduce this role, we need to understand the contributions of both kinds of afferents to central processing, a topic we will consider in Chapter 7.

A more detailed treatment of information transmission is found online ("Information Theory in the Vestibular System").

4.2 SEMICIRCULAR CANALS

Canals and otolith organs differ in their functions: the former sense angular rotations, while the latter monitor linear motions and head tilts. Consistent with this conclusion, canal afferents respond to angular head rotations. In acute

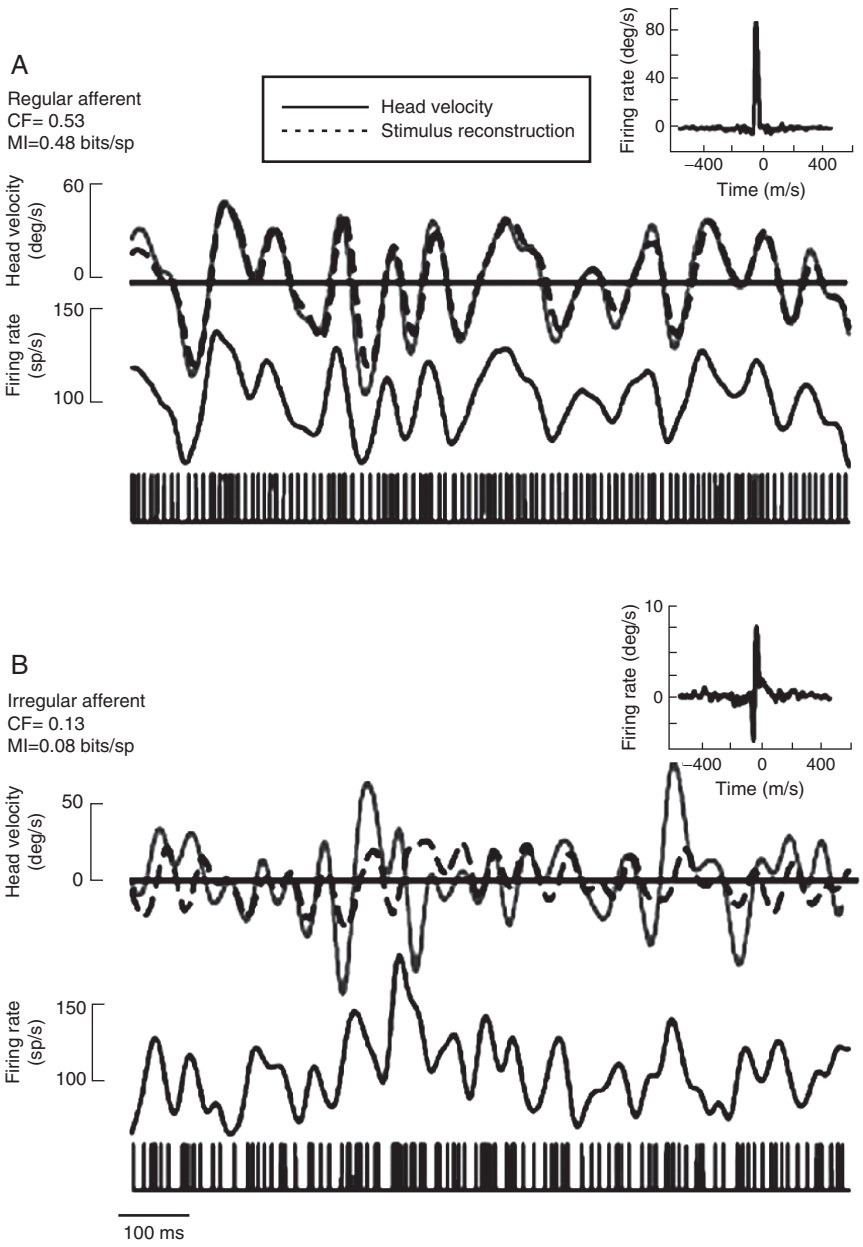

Figure 4.6 Stimulus reconstructions for two horizontal semicircular canal units to rotational broadband (0 to 20 Hz) Gaussian pseudorandom stimulation. Time-dependent firing rates (*lower trace*) are shown for a regular (**A**) and an irregular unit (**B**). For each unit, an impulse response (see *insets*), when convolved with the spike train, gave a reconstructed stimulus that minimized the error between the reconstruction and the actual stimulus (*upper trace*). The regular unit provided a more faithful reconstruction. *CF*, coding fraction; *MI*, mutual information. (From Sadeghi et al. 2007a)

preparations these same afferents can also respond to linear forces (Estes et al. 1975; Goldberg and Fernandez 1975; Perachio and Correia 1983). One interpretation of the linear-force responses is that they are artifacts caused by thermal or other gradients introduced into the endolymphatic ring by the acute exposure of the temporal bone (Goldberg and Fernandez 1975). Consistent with this hypothesis, such responses are not found when less invasive recordings are made in chronic animals (Correia et al. 1992; Somps et al. 1994).

Directional Properties

From physical principles, it would be expected that in response to head rotations the displacement of endolymph in each canal duct would be proportional to the cosine of the angle between an optimal plane and the plane of motion. Were fluid flow in each of the three canals independent of one another, the optimal plane should correspond to the geometric canal plane. But because each canal has two openings into the utriculus, fluid flows in the three canals are not independent and the optimal planes can deviate from the geometric planes (Rabbitt 1999). Detailed anatomical measurements of canal planes are available for several species (Blanks et al. 1972, 1985; Curthoys et al. 1975; Reisine et al. 1988). Experimentally, the optimal planes, measured from afferent discharge, are within 10 degrees of the geometric planes (Estes et al. 1975; Haque et al. 2004; Reisine et al. 1988).

Ewald (1892) studied directional properties by applying or removing pressure from canal ducts while monitoring head and eye movements. He summarized his finding in two laws: responses were in the plane of the stimulated canal (First Law) and one stimulus direction (push or pull) led to distinctly larger responses in each canal (Second Law). Afferent recordings (Lowenstein and Sand 1940a) paralleled Ewald's findings. All afferents innervating a given canal have the same directional properties. Deflections of the cupula toward the utriculus are excitatory for the horizontal canal and inhibitory for the vertical canals. Excitatory directions are those that led to larger responses in Ewald's experiments, and they correlated with hair-bundle morphological polarization, which is uniform in each crista (see Fig. 2.9C), but oppositely directed in the horizontal and vertical cristae (Lindeman 1969; Lowenstein and Wersäll 1954). The canals are arranged in coplanar pairs with the two horizontal canals forming a pair, as do the anterior canal on one side and the contralateral posterior canal (see Fig. 2.3). Based on the particular canals (A, H, P) and the side of the head (L, R), the three pairs are referred to as LHRH, LARP, and RALP. Any head rotation causing excitation or inhibition from a canal will result in an oppositely directed response from the contralateral coplanar canal. It is the difference in discharge between coplanar canals that is interpreted by the brain as a head rotation.

Macromechanics and the Torsion-Pendulum Model

Early workers (Breuer 1874, 1875; Crum Brown 1874; Mach 1874) speculated that the semicircular canals, because of their toroidal topology, were involved in sensing rotational head movements. The nerve endings in the canal were presumed to be sensitive to fluid pressure (Mach 1874) or fluid motion (Crum Brown 1874; Breuer 1874). There was a difficulty with these theories. Pressure or motion in an unoccluded canal should outlast head movements by only a few milliseconds. Yet, it was known that vestibular reflexes and sensations can persist for many seconds following certain motion profiles, for example when a subject on rotating platform is suddenly stopped after a period of constant angular velocity. Two explanations could be offered for the apparent discrepancy between fluid motion and the central manifestations of canal excitation: (1) biomechanical models of the canals were deficient or (2) central mechanisms could result in a perseveration of the activity triggered by afferent input. As it turns out, both peripheral and central mechanisms are involved in prolonging vestibular responses. The central mechanisms are termed "velocity storage" and will be considered later (Chapters 9 and 11). Here, we concentrate on peripheral mechanisms.

Classical theories ignored the influence of the cupula on fluid motion. A reason for this misconception was the shrinkage of the cupula during histological fixation. To appreciate the role of

the cupula, it had to be visualized *in situ* without fixatives. This was done by Steinhausen (1931), who injected dye into the unfixed membranous labyrinth of fish. He discovered that the cupula, rather than sitting atop the crista like a cocked hat, extended across the lumen from the top of the crista to the vault of the ampulla, where it formed a hydraulic seal. In response to rotations, the cupula was observed to move across the ampullary vault like a "swinging gate." Importantly, when the cupula was displaced, it was observed to take several seconds to return to its neutral position. Dohlman (1935) confirmed Steinhausen's observations. Later studies found that the cupula, rather than moving like a "swinging gate," is tethered both to the vault of the ampulla and to the crista and moves like a diaphragm constrained along its entire circumference (Hillman and McLaren 1979).

Steinhausen (1931) not only provided evidence for the role of the cupula but also developed a quantitative model of the macromechanics. The model is formally similar to a torsion pendulum, such as illustrated in textbooks of elementary physics. In the model, excitation is assumed to be proportional to the displacement of the cupula-endolymph relative to the canal wall. The original model, as well as subsequent versions (Jones and Spells 1963; Ramprashad et al. 1984; van Egmond et al. 1949), treated the canal duct similarly, but differed in the way they handled the enlarged volumes of the ampulla and utricular sac. The first model to deal satisfactorily with this complex geometry treated the mechanics in a piecewise manner (Oman et al. 1987).

As in other versions of the torsion-pendulum model, the piecewise model leads to a second-order differential equation that relates the angular acceleration of the head, α to the displacement of the endolymph in the canal duct (x_{CD}). Three factors determine the relation: (1) the geometry of the canal, in this case its radius of curvature, $R(l)$, and its cross-sectional area, $A(l)$, both expressed as functions of l, the position along the streamline (Fig. 4.7A); (2) the physical properties of the endolymph, including its density, ρ, and viscosity, μ; and (3) the elasticity of the cupula (k). To simplify the geometry, we assume that the centerline of the canal is a circle of radius, R, and that the canal duct (CD) has a constant cross-sectional area, A_{CD}, and a length, L_{CD}. The entire centerline, including the ampulla and the utriculus, has a length, L.

To deduce the model's behavior, we consider the forces acting on dl, an infinitesimal segment of the endolymph in the canal duct (Fig. 4.7B). The theory leads to the second-order equation

$$\rho\ddot{Q}\oint_{L_{CD}}\frac{dl}{A(l)}+8\pi\mu\dot{Q}\oint_{L_{CD}}\frac{dl}{A^2(l)}+kQ = -\rho\oint_{L}a_X(l)\,dl \qquad (4.1)$$

where Q is the volume displacement of the endolymph, the line integrals are calculated over the entire length of the streamline, and $a_X(l) = R\langle_X(l)$, where $a_X(l)$ is the linear acceleration equivalent to $\langle_X(l)$, the component of head angular acceleration in the canal plane. To denote derivatives, we use the dot convention, $\dot{Q} = dQ/dt$ and $\ddot{Q} = d^2Q/dt^2$. Because of fluid continuity, Q is the same across any cross-section, including the cupula, in which case $Q = A_{CD}x_{CD} = A_{CUP}x_{CUP}$. Here, x_{CD} and x_{CUP} are the linear displacements in the canal duct (CD) and the cupula (CUP), respectively; A_{CD} and A_{CUP} are the corresponding cross-sectional areas. $A(l)$ is much smaller in the canal duct than in the cupula and the utriculus. As a result, the first two terms on the left side need to be evaluated only over the length of the canal duct, L_{CD} A derivation of the equation can be found online ("Torsion pendulum"). The equivalent lumped model is depicted in Figure 4.7C.

We will use Equation 4.1 to deduce the response of the cupula to head rotations. But we first consider why the canals do not respond to linear forces. When there is an angular acceleration, there is a net couple, $-\rho LR\alpha\cos\theta$ that moves the endolymph. Now consider a linear acceleration, $\boldsymbol{a}^{\mathbf{x}}$, that is constant in magnitude and direction. Here, the couples at points 180 degrees apart will cancel. As a result, the net couple will vanish and there will be no movement of the cupula and endolymph. While cancellation does not depend on the exact geometry of the canal, it does depend on the density of the endolymph being constant along its entire length (L).

A variable density provides a basis for the caloric response in which hot or cold water is flushed into the ear canal and changes the density of endolymph in the external-most part of

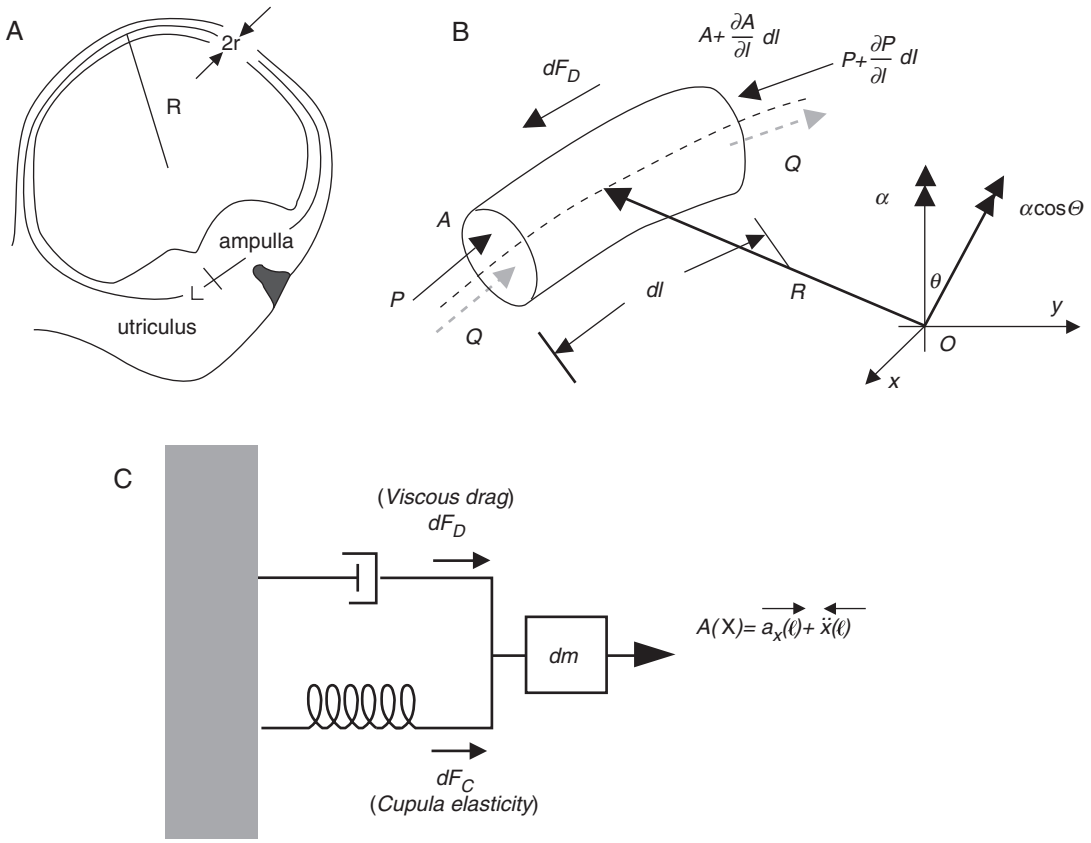

Figure 4.7 **A**. Planar section of the membranous semicircular canal. *R*, radius of curvature; *r*, cross-sectional radius of canal duct. Streamline has a length, *L*. (Modified from Curthoys and Oman 1986 **B**. Free-body diagram of an infinitesimal section of the canal duct of length, *dl*, and cross-sectional area, *A*. *Q*, volume flow of endolymph. Fluid pressure, *P*. dF_D, force on fluid due to viscous drag. α, angular acceleration of the head in a plane tilted at an angle, θ, from the effective canal plane. The component of linear acceleration of the head in the canal plane is Rα cos θ. (Modified from Rabbitt et al. 2004a) **C**. A lumped model of macromechanics. As the head is accelerated in space, $\vec{a}_x(\ell)$, endolymph accelerates backward relative to the canal wall, $\ddot{\vec{x}}(\ell)$. The backward movement is opposed by two restoring forces, the viscous drag exerted by the canal wall (dF_D) and the elasticity of the cupula (dF_C).

the horizontal-canal duct. Placing a subject in a supine position allows gravity to act in the plane of the horizontal canal. With warm water in the ear canal, endolymph in the canal duct becomes less dense and will rise under the influence of gravity. The result is a buoyant force that should move the cupula towards the utriculus and, hence, is excitatory. Cold water produces the opposite reaction: cupular displacement is towards the canal duct and is inhibitory. Afferent recordings confirm that the canal becomes sensitive to linear forces during caloric stimulation (Young and Anderson 1974). While the caloric response was recognized in the 19th century (Goltz 1870), Bárány (1906) is credited with the realization that at least part of the response is due to the buoyancy of endolymph. There are also non-buoyancy components (Coats and Smith 1967; Minor and Goldberg 1990; Paige 1985), as was convincingly demonstrated by the persistence of a caloric response during spaceflight (Scherer et al. 1986). Non-buoyancy

components could include direct temperature effects on various stages of transduction and/or temperature-dependent localized expansions and contractions of labyrinthine fluids, which could result in a cupular displacement (Scherer and Clarke 1985). We will come back to this topic in Chapter 16.

Returning to rotational stimulation, we note that Equation 4.1 is a second-order, linear ordinary differential equation of the form

Au:- Please check if this equation is okay?

$$M\ddot{x} + B\dot{x} + Kx = -f(t) \quad (4.2)$$

The behavior of the equation is determined by two time constants. As we shall see, $B^2 >> 4MK$, in which case the system is overdamped and the time constants can be evaluated as

$$\tau_1 = B/K = \frac{8\pi\mu L_{CD}}{kA_{CD}^2} \quad (4.3)$$

and

$$\tau_2 = M/B = \frac{\rho A_{CD}}{8\pi\mu} \quad (4.4)$$

with $\tau_1 >> \tau_2$ Substituting these values of the time constants into Equation 4.2 gives

$$\ddot{x} + \dot{x}/\tau_2 + x/\tau_1\tau_2 = -R(f_A/f_L)\alpha\cos\theta \quad (4.5)$$

where x is average cupular displacement. Here, $f_A = A_{CD}/A_{CUP}$, $f_L = L/L_{CD}$, and the subscripts (CD and CUP) refer, respectively, to the canal duct and the cupula.

Equation 4.5 can be solved by standard methods (see, for example, Edwards and Penney 2000). One such method, Laplace transforms, is considered online ("A Primer on Integral Transforms"). To illustrate the workings of the equation, we show solutions for two head movements. The first is a brief motion that might occur during a voluntary head saccade intended to bring a target located in the visual periphery into the center of gaze (Fig. 4.8A). Here, the magnitude of cupular position almost exactly parallels angular head velocity. In the second example, angular velocity is gradually built up and then the motion is abruptly stopped (Fig. 4.8B). As velocity grows, cupular displacement increases in an exponential manner, its magnitude initially paralleling angular velocity, but eventually reaching an asymptote proportional to angular acceleration. When the motion is stopped, the cupula is flung in the opposite direction and only slowly returns to rest. While the stimulus in Figure 4.8A resembles a typical, everyday voluntary head movement, the motion in Figure 4.8B is atypically slow and the terminal deceleration is atypical in not being matched by

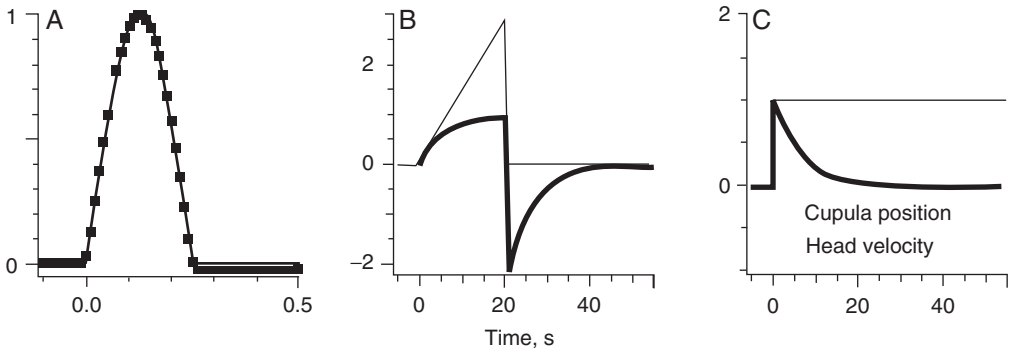

Figure 4.8 Solution of the torsion-pendulum equation (*thick dots* in **A** and *thick lines* in **B** and **C**) for three angular head-velocity profiles (*thin lines*). In all calculations, long time-constant, $\tau_1 = 5$ s. **A**. A brief rotation consisting of the excitatory half-cycle of a 2-Hz sine wave. The response magnitude parallels the rotation profile. **B**. A velocity ramp (acceleration step) lasting 20 s, followed by a sudden stop. The response consists of an exponential build-up, a large displacement in the opposite direction, followed by an exponential return to the baseline. **C**. A velocity step leads to a transient exponential response after an initial step. In all cases, cupular deflection was inverted to facilitate comparison with head velocity.

an immediately preceding, oppositely directed acceleration of similar magnitude. Interest in the latter motion stems in part from its historical use in clinical vestibular testing and in part because it mimics a playground maneuver (see Chapter 1.4). While a voluntary head movement cannot accomplish the motion, it can be obtained by whole-body spins on a turntable or by self-generated spinning. As the reader was asked to verify in Chapter 1, the brief deceleration terminating the motion can lead to vertigo and postural instability. Later in this chapter, we will see that afferent discharge more or less parallels cupular displacement and that the brain interprets the discharge as proportional to angular head velocity. During the later parts of the rotation and particularly in the post-rotatory period, cupular displacement and afferent discharge no longer indicate true angular head velocity and will be in conflict with information provided by vision and proprioception. This is an example of the conclusion, stated in Chapter 1, that vertigo arises when there is a conflict or mismatch between different sensory channels. In contrast, the motion depicted in Figure 4.8A is unaccompanied by such symptoms, reflecting the fact that cupular displacement is congruent with head velocity and non-vestibular inputs.

The relation between head movements and cupular displacement can be summarized by a so-called Bode plot, in which the gain and phase of cupular displacement is plotted as a function of sinusoidal frequency (Fig. 4.9). In the figure, vertical dashed lines are drawn at the two

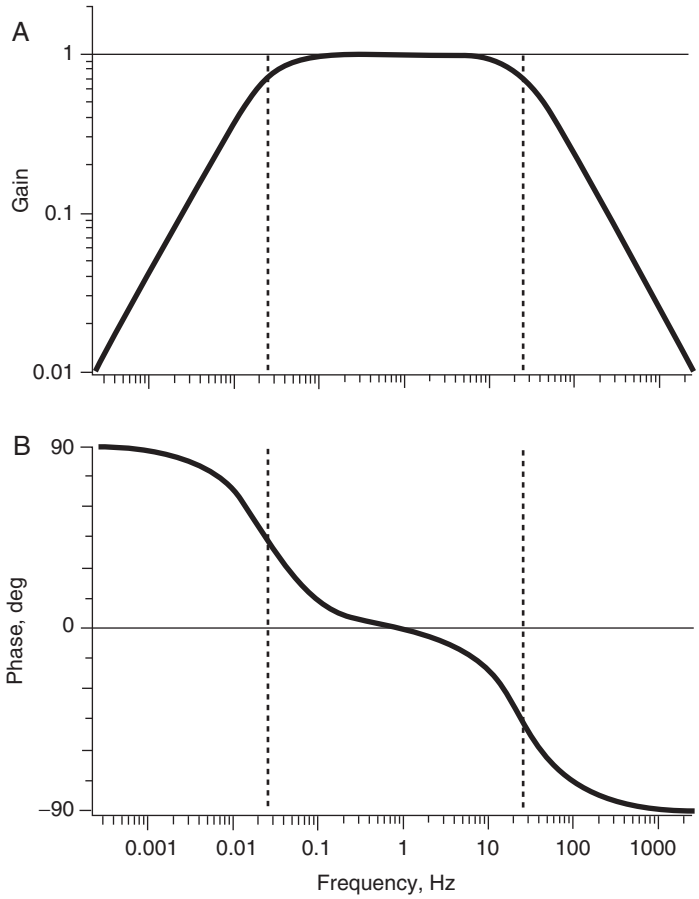

Figure 4.9 Bode plot of torsion-pendulum model, including gain (**A**) and phase (**B**) re angular head velocity. Corner frequencies, 0.025 and 25 Hz. *Vertical dashed lines* divide the spectrum into low-, mid-, and high-frequency regions in which the output parallels angular acceleration, velocity, and displacement, respectively.

so-called corner frequencies, $f_1 = 1/2\pi\tau_1$ and $f_2 = 1/2\pi\tau_2$, related to the time constants of Equation 4.5. The lines divide the frequency axis into a low-frequency region ($f < f_1$), a mid-frequency region (between f_1 and f_2), and a high-frequency region ($f > f_2$). In the low-frequency region, the system is an acceleration transducer: gain re velocity increases in proportion to f, which is equivalent to a constant gain re acceleration, and the phase lead re velocity approaches 90 degrees, in register with acceleration. The system approximates a velocity transducer in the mid-frequency range: gain re velocity is nearly constant and phase re velocity is near 0 degrees. In the high-frequency region, the system becomes a displacement transducer: gain re velocity is inversely proportional to frequency and phase re velocity approaches a 90-degree lag, which places response in phase with head displacement. These three regimes reflect the three terms on the left side of Equation 4.5 corresponding to the influence of endolymph mass ($M\ddot{x}$), endolymph viscosity ($B\dot{x}$) and cupular elasticity (Kx). As sinusoidal frequency is lowered from high values, the system is dominated first by the mass term, then by the viscous term, and finally by the elastic term. The right-hand side of the equation remains proportional to angular head acceleration (α). A solution in terms of cupular displacement (x) requires a double integration of α when the mass term dominates, a single integration when the viscous term dominates, and no integration when the elastic term dominates.

The mid-frequency region or midband extends over three decades. Typical voluntary head movements fall comfortably within the midband (Armand and Minor 2001; Liao et al. 2005), as do the head perturbations accompanying locomotion (Grossman et al. 1988) and other daily activities (MacDougall and Moore 2005). Most of the energy in such head movements falls in a frequency band from 0.5 Hz to possibly 20 Hz, with a peak around 2 to 5 Hz. For such head movements, the semicircular canals function as angular-velocity transducers. To see how the brain interprets neural signals emanating from the canals, we can consider the eye movements produced during vestibular stimulation. As will be considered in Chapter 9, it is the velocity of eye movements that parallels cupular displacement. Psychophysical studies indicate a similar parallel when the sensation of turning is estimated by the subject (Guedry 1974). From both its macromechanics and the way the brain interprets its signals, the semicircular canals function as sensors of angular velocity for midband frequencies.

The restriction to midband frequencies is important since at very low frequencies the canals serve as angular-acceleration transducers. This makes physical sense since only head accelerations result in the inertial forces that produce fluid motion. It is the reactive forces resulting from fluid motion, including endolymph viscosity and cupular elasticity, that determine stimulus specificity. These ideas can be illustrated by the response of the cupula-endolymph to a prolonged step of angular velocity (see Fig. 4.8C). There is a response at the beginning of the step, which decays exponentially with a time constant of about 5 s. Unlike the situation for a constant head acceleration (see Fig. 4.8B), there is no steady-state response, which is why we do not sense the rotation of the earth about its axis or around the sun.

The torsion-pendulum model can be used to compute cupular displacements for the dynamic range over which the semicircular canals operate. Based on studies in humans, the threshold for detection of long-duration head accelerations is near 0.1 deg/s^2 (Clark 1967; Guedry 1974). From voluntary head movements in humans, a large, typically encountered rotation can be taken as 400 deg/s (Armand and Minor 2001; Liao et al. 2005). From the torsion-pendulum equation, we can compute the average displacement of the cupula for long-duration accelerations (Oman and Young 1972). By assuming that the cupula adopts a parabolic shape, we can calculate the displacement immediately above the crista, at a distance corresponding to the average height of the tallest stereocilia. In the center of the crista, the height is 5 to 10 μm, whereas at the periphery of the neuroepithelium, hair bundles can be much longer (Lewis et al. 1985; Lim 1976). The calculated displacement of central stereocilia at threshold is 1.5 to 3 nm, about 1% to 2% the diameter of an individual stereocilium (Hunter-Duvar and Hinajosa 1984). For a 400 deg/s midband rotation, the calculated central hair-bundle displacement is 0.6 μm,

within the dynamic range for mechanoelectric transducer (MET) currents in some vestibular hair cells (Holt et al. 1997). At threshold, the pressure across the cupula is 1×10^{-3} dyne/cm^2.

The numbers emphasize both the sensitivity and the versatility of the organ. Calculated threshold displacements and pressures are similar in magnitude to those obtained in the mammalian cochlea at hearing threshold (Olson 2001; Robles and Ruggero 2001). At the other end of the amplitude scale, evidence from afferent recordings indicates that the cupular or hair-bundle displacements occurring during large head rotations do not challenge the structural integrity of the transduction machinery.

Interspecies Variations and Canal Dimensions

Several of the parameters appearing in the torsion-pendulum model (Equation 4.5) are related to the dimensions of the semicircular canal. So, for example, average cupular displacement, x, re angular head velocity, ω, for mid-band head rotations is

$$x = -\frac{p\left(f_A / f_L\right) Rr^2}{8\mu}\omega \qquad (4.6)$$

where R is the radius of curvature and r is the cross-sectional radius of the canal duct. At a constant temperature, the physical constants, ρ and μ, are fixed and the ratios, f_A and f_L, are nearly constant across species, so, to a first approximation, sensitivity (x/ω), should be proportional to the product, Rr^2.

Relations between torsion-pendulum parameters and canal geometry (van Egmond et al. 1949) were exploited by Melvill Jones (Jones and Spells 1963; Melvill Jones 1974), who compared the value of Rr^2 across species. In mammals, Rr^2 increased 20-fold over a 10^5 range of body weights. Melvill Jones speculated that the increase in sensitivity with body mass reflected an adaptive matching of canal sensitivity to movement repertoire. Furthermore, it was suggested that the frequencies defining the mid-band should move downward with body mass. In general, large animals, being more sluggish than small animals, would benefit from an increase in canal sensitivity. The downward shift of the midband was interpreted as matching canal dynamics to the slower movements of large animals. To determine whether sensitivity changes in the manner suggested by Melvill Jones (Jones and Spells 1963; Melvill Jones 1974), we can compare for several species experimental values, obtained from afferent recordings, with values predicted from canal geometry (Fig. 4.10) (see Yang and Hullar 2007). In all cases, gains were confined to regular units. Except possibly for the cat, there is reasonable agreement between empirical gains and the predictions of the Jones-Spells theory.

While the agreement is reassuring, some of the assumptions implicit in the theory require comment. First, it was tacitly assumed that any particular canal has a single sensitivity. In mammals, there is an approximately 10-fold variation

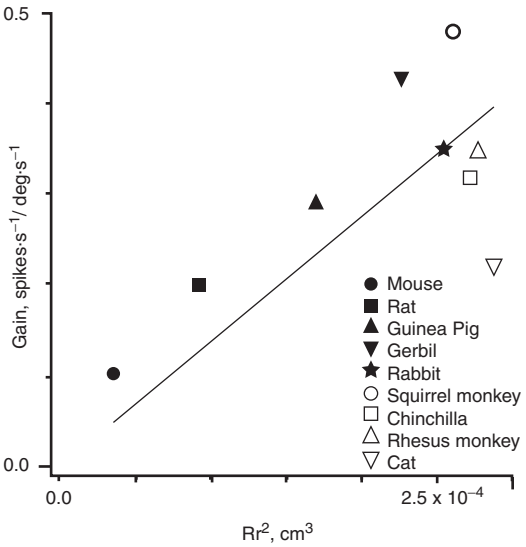

Figure 4.10 Relation between the mean rotational gain of regular semicircular canal afferents (cv* < 0.10) and the dimensions of the membranous canal. *R*, radius of curvature; *r*, cross-sectional radius of the membranous canal duct. Line is best-fitting regression passing through the origin. Morphological data, mouse (Calabrese and Hullar 2006; A Lysakowski, personal communication); rat, guinea pig (Curthoys and Oman 1986); gerbil, rabbit, chinchilla (Ramprashad et al. 1984); squirrel monkey, cat (Igarashi 1967); rhesus monkey (Jones and Spells 1963). Physiological data, mouse (Yang and Hullar 2007); rat, guinea pig (Curthoys 1982); gerbil (Schneider and Anderson 1976); rabbit (Stahl 1992); squirrel monkey (Lysakowski et al. 1995); chinchilla (Baird et al. 1988); rhesus monkey (Haque et al. 2004); cat (Tomko et al. 1981b).

in afferent sensitivity systematically related to discharge regularity (Baird et al. 1988; Curthoys 1982; Goldberg and Fernandez 1971b; Haque et al. 2004; Lysakowski et al. 1995; Ramachandran and Lisberger 2006; Sadeghi et al. 2007b; Schneider and Anderson 1976; Tomko et al. 1981b). An even larger, almost 100-fold variation in afferent sensitivity is seen in lower vertebrates (Boyle and Highstein 1990; Brichta and Goldberg 2000a; Honrubia et al. 1989). Much of the gain variation seen in mammals can be ascribed to differences in encoder sensitivity (see Section 4.1, Discharge regularity), implying that macromechanics is not a limiting consideration. Second, Melvill Jones suggested that variations in time constants could be used to match canal dynamics with the dynamics of head motions. But the bandwidth of typical head movements is much narrower than the canal midband, in which case the hypothesized dynamic matching would be of marginal adaptive value. Furthermore and contrary to predictions, when closely related animals are compared, canal dimensions tend to be larger in the more agile species (reviewed in Spoor 1998). Third, the variation in the dimensions of the vestibular end organs may reflect constraints other than those related to the presumed need to match afferent signals to head movements—for example, the need to fit the labyrinth into different-sized skulls or to innervate the vestibular nuclei whose size grows with body mass (Matano 1986; Stephan et al. 1981).

Afferent Response Dynamics

Do dynamics parallel the torsion-pendulum model or are they modified by any of the several stages of vestibular transduction interposed between macromechanics and afferent-nerve discharge? To study the question, we can examine afferent responses to sinusoidal head rotations. But first we need to determine whether the system behaves linearly as would be consistent with the linear differential equation defining the torsion-pendulum model (Equation 4.1). As illustrated in Figure 4.11, responses resemble those of a linear system in three ways. First, there is no evidence of a threshold or discontinuity as the curves pass through zero response. Second, responses are close to sinusoidal with nonlinear distortions typically less than 10%. Much of the nonlinear distortion reflects asymmetries between excitatory and inhibitory responses. Third, gains and phases at a given frequency are almost constant as peak velocity varies over a wide range (Fig. 4.11 inset).

Gains and phases for typical regular and irregular afferents are compared in Figure 4.12 with those expected from macromechanics. Data are from the squirrel monkey (Fernández and Goldberg 1971; Goldberg and Fernandez 1971b). Throughout a frequency range extending up to 0.5 Hz, the gains and phases of the regular afferent are close to those expected from the torsion-pendulum model, but above 0.5 Hz, there are discrepancies. The irregularly discharging afferent shows deviations from expected values at both low and high frequencies.

Consider the high-frequency deviations. As frequency is increased above 0.5 Hz, there are progressive phase leads and gain enhancements not predicted by the torsion-pendulum model. Deviations are larger in the irregular unit and can be interpreted as indicating that afferent response, r(t), is proportional to a weighted sum of cupular displacement, x(t), and velocity, dx/dt, with the relative weight of the two factors varying across units, but not with frequency. That is, afferent response

$$r(t) \propto x(t) + \tau_V dx/dt \qquad (4.7)$$

In the formulation, x(t) is the expected response based on the torsion-pendulum model and τ_V is a fixed weight characteristic of each afferent. The larger the weight, the more conspicuous is the velocity term. Equation 4.7 describes the high-frequency deviations in both units of Figure 4.12. In the irregular unit, $\tau_V = 0.080$ s provides a best fit to the data. Even though the discrepancy is smaller in the regular unit, it can be fit by Equation 4.7 with a value of $\tau_V = 0.015$ s. That the differences in response dynamics of afferents can be described by the variation of one or a few parameters in a transfer function may be termed *parameterization*. A practical consequence of parameterization is that differences between units can usually be characterized by determining their gains and phases at a single frequency. Parameterization holds for afferents recorded in mammals other than the squirrel monkey, even though the

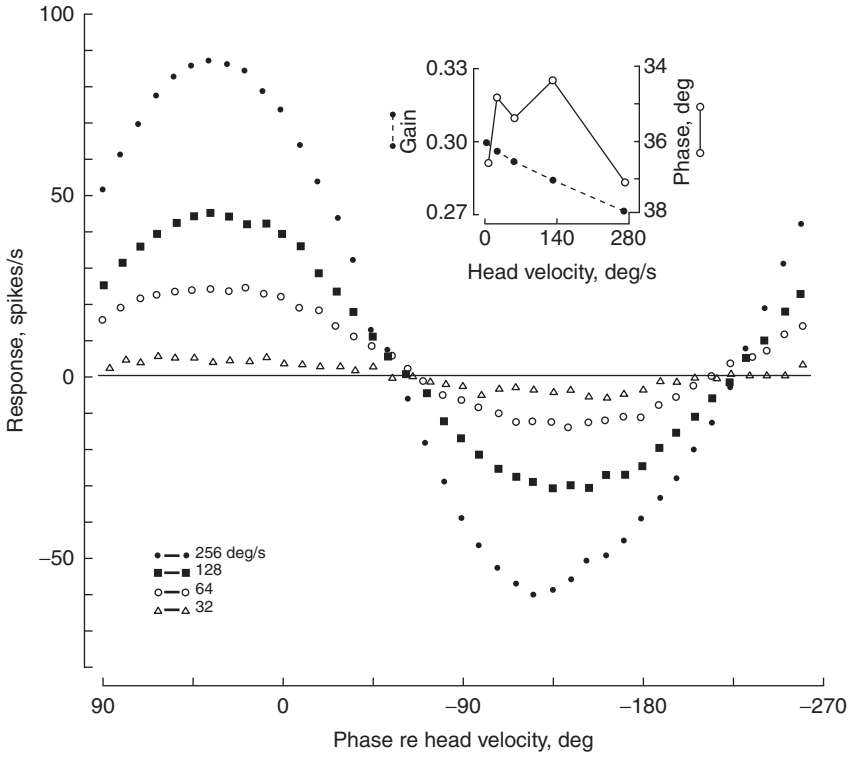

Figure 4.11 Steady-state sinusoidal responses of the same anterior canal unit as in Figure 4.1 to 0.05-Hz sinusoidal head rotations different peak angular velocities. Responses are sinusoidal in form and do not show a discontinuity on passing from excitation to inhibition. Zero degrees, peak excitatory velocity. Response leads stimulus. *Inset* plots gain and phase re head velocity as functions of peak velocity. Both gains and phases are almost constant even though stimulus magnitude changes 16-fold (*inset*). (From Fernández and Goldberg 1971)

high-frequency velocity sensitivity may involve fractional operators (Baird et al. 1988; Curthoys 1982; Schneider and Anderson 1976; Tomko et al. 1981b), rather than the integral operator used in Equation 4.7.

We now consider the low-frequency deviation. This is best seen in the responses to long-duration angular-velocity trapezoids, which are shown for a regular unit (Fig. 4.13A) and an irregular unit (Fig. 4.13B). Except for an asymmetry between its excitatory and inhibitory responses, the regular unit conforms to expectations from the torsion-pendulum model. During long-duration constant angular accelerations and decelerations, excitatory and inhibitory responses build up exponentially with time constants near 5 s. The return to the resting discharge from either kind of response is also exponential. In contrast, the discharge of the irregular unit shows per-acceleratory response declines and post-acceleratory secondary responses, including an undershoot in rate following excitation and an overshoot following inhibition. Adaptation is also reflected as phase leads in the response to very low-frequency (≤0.025 Hz) sinusoidal head rotations (Fernández and Goldberg 1971) (see Fig. 4.12).

What mechanisms contribute to differences between afferents in their response dynamics? Conceivably, any of the transduction steps interposed between head motion and afferent discharge may contribute to afferent diversity. Two complementary strategies have been used to identify potential mechanisms: (1) electric

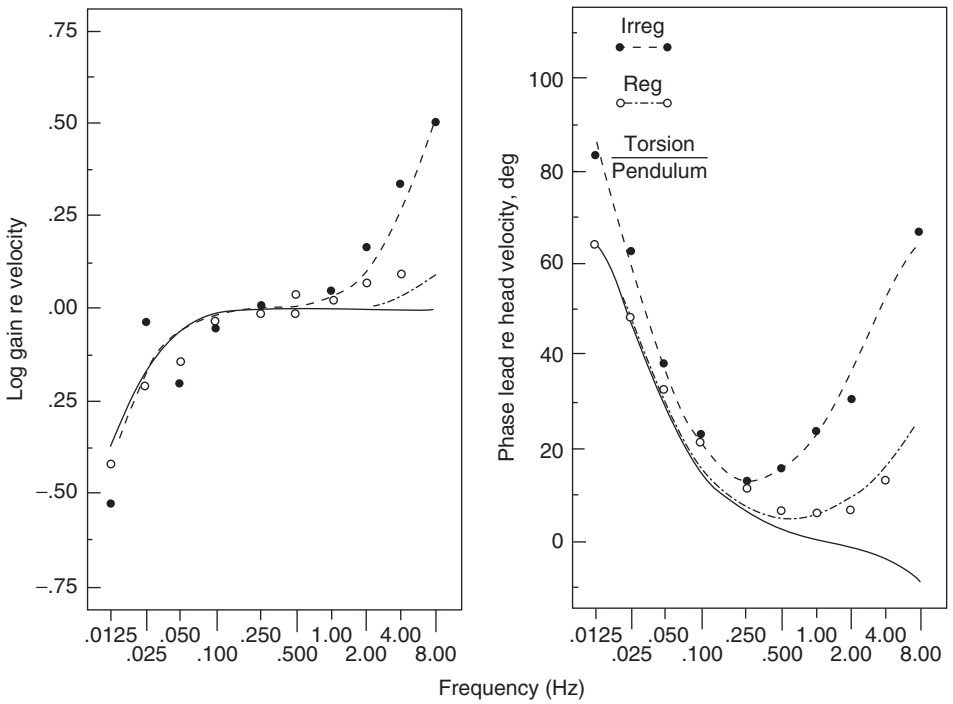

Figure 4.12 Response dynamics of semicircular-canal afferents in the squirrel monkey. Because their responses are nearly linear, the afferents can be characterized by their gains (*left*) and phase leads (*right*) re angular head velocity in response to sinusoidal head rotations. Such Bode plots are compared for an irregular (*Irreg,*) unit, a regular (*Reg*) unit, and the torsion-pendulum model. (From Goldberg and Fernández 1971b)

currents have been used to bypass various transduction stages and (2) recordings have been made from hair cells and afferent terminals to distinguish contributions at various stages of the trandusduction chain.

Cupular Deflection

While there may be a differential displacement between the center and planar edges of the cupula, the effect is likely to be small and confined to relatively high frequencies (Highstein et al. 2005; Rabbitt et al. 2004a). The reasoning is confirmed in mammals; here there is a concentric organization of the crista such that regularly discharging afferents with indistinguishable response dynamics are found throughout the peripheral zone, including the base of the crista along its longitudinal length and the apex near the planum semilunatum (Baird et al. 1988). This observation suggests that regional variations in cupular mechanics are unlikely to make a major contribution to the diversity of response dynamics seen in mammals.

Hair-Bundle Micromechanics

Hair bundles are shorter in central/striolar zones than in peripheral/extrastriolar zones (Lewis et al. 1985). A looser or viscous coupling between the shorter bundles and the overlying accessory structure might contribute to the more phasic response dynamics of central/striolar afferents. Here, the evidence is contradictory. Mechanical stimulation of semicircular canals has been compared with electrical polarization of the endolymphatic space in the toadfish (Highstein et al. 1996). Presumably, hair-bundle deflections are involved in the responses to mechanical but not to galvanic stimulation. The two modes of stimulation had different effects on the most tonic and most phasic afferents,

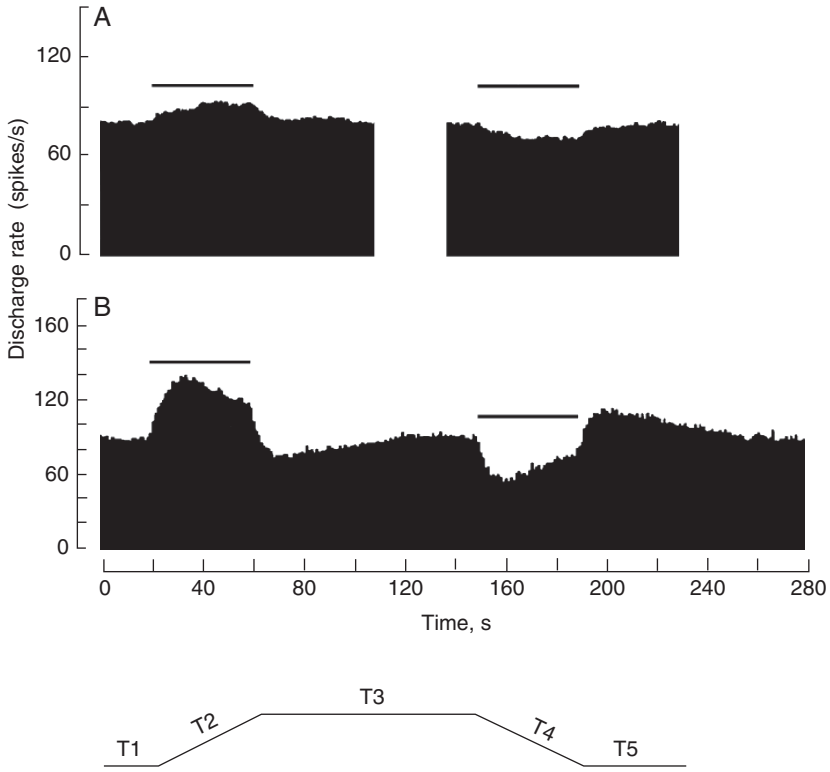

Figure 4.13 Some afferents show a low-frequency adaptation, which can be demonstrated with velocity trapezoids, in this case consisting of two 40-s velocity ramps (acceleration, 7.5 deg/s^2) separated by a 60-s (**A**) or a 90-s (**B**) velocity plateau. An irregular unit (**B**) shows adaptation, which consists of per-stimulus response declines and post-stimulus secondary responses. A regular unit (**A**) shows little adaptation as its response increases exponentially during velocity ramps and decreases exponentially during the velocity plateau. There is a 30-s break in **A** so that the inhibitory ramps for the two units are in register. The velocity profile is shown below and consists of a rest period (*T1*), an excitatory velocity ramp (*T2*), a velocity plateau (*T3*), an inhibitory velocity ramp (*T4*), and a final stationary period (*T5*). (From Goldberg and Fernández 1971a)

consistent with a micromechanical contribution to response dynamic diversity.

Hair-cell recordings of receptor potentials in the toadfish crista during mechanical stimulation have led to a different conclusion (Highstein et al. 1996). Here, sinusoidal stimulation resulted in relatively flat (tonic) response dynamics. Furthermore, there was relatively little adaptation to step stimulation. Taken at face value, the results would imply either that the hair cells sampled only supplied tonic afferents or else that micromechanics do not contribute to dynamic diversity. But as the authors themselves point out (Highstein et al. 1996), the results should be interpreted cautiously. In particular, recordings with sharp electrodes may distort hair-cell physiology.

Transducer Ddaptation

The decline in transducer currents during sustained hair-bundle deflections is an obvious candidate for shaping response dynamics. Yet, here too results are not entirely consistent. Work has been done in the utricular macula where striolar afferents have more phasic response dynamics than extrastriolar afferents. Recordings in early postnatal mice did not show any differences in adaptive properties between striolar and extrastriolar hair cells (Vollrath and Eatock 2003).

In contrast, striking differences were seen in or near the striola of the frog utriculus among hair cells differing in bundle morphology (Baird 1994).

Basolateral Currents

Such currents, by shaping receptor potentials, could contribute to the response dynamics of hair cells. Despite the large repertoire of such currents (Eatock and Lysakowski, 2006; Guth et al. 1998), it is unlikely that they contribute to the diversity of afferent response dynamics. The negative conclusion is based on comparisons between two populations of hair cells in the turtle posterior crista, those near the center (torus) and those near the edge of the organ (planum). Despite large differences in afferent response dynamics (Brichta and Goldberg 2000a), the two sets of hair cells were indistinguishable in the gains and phases of their current-clamp responses to sinusoidal currents (Goldberg and Brichta 2002b). It should be noted that the results were obtained in enzymatically dissociated hair cells and might be different *in vivo*.

Quantal Release

As we saw in Chapter 3, neurotransmitter is released from hair cells in quantal packets. The sinusoidal modulation of quantal rate presumably reflects presynaptic mechanisms. By comparing quantal release to spike discharge, we can estimate the hair-cell (presynaptic) and afferent-terminal (postsynaptic) contribution to response dynamics. This has been done in the turtle posterior crista (Holt et al. 2006b). Figure 4.14A, based on the response of a single unit to canal-duct indentation at 0.3 Hz, compares variations in spike rate and quantal rate over a single cycle. The stimulus has an excitatory peak at 270 degrees (vertical bar). Spike activity leads the mechanical stimulus by 66 degrees (red curve), about 35 degrees more phase advanced than quantal activity (blue curve). Were there complete agreement between the spike and quantal phases, this would suggest that the spike phase is entirely determined by presynaptic (hair-cell) mechanisms. A postsynaptic contribution is suggested by the 35-degree discrepancy between the two curves.

Comparisons for a population of afferents are seen in Figure 4.14B. There is a strong correlation between spike and quantal phases. At the same time the discrepancy between the two phases grows, the larger are the phase leads or, equivalently, the more phasic the response dynamics. About two thirds of the total variation in spike phase can be ascribed to quantal phase and is likely, therefore, to be caused by presynaptic factors. The data do not allow us to specify the presynaptic factors involved, which may include any of the several mechanisms described above. One mechanism considered in Chapter 3 is vesicle turnover. It would be expected that there would be a depletion of vesicles during excitation and their replenishment during inhibition. Both effects would lead to a phase advance. Such processes may underlie adaptation in the fish sacculus (Furukawa and Matsuura 1978; Furukawa et al. 1982) and in chick (Spassova et al. 2004) and mammalian auditory afferents (Goutman and Glowatzki 2007).

Postsynaptic Mechanisms

As illustrated in Figure 4.14B, about one third of the phase variation across units cannot be accounted for by presynaptic mechanisms. This fraction may be due to any of several postsynaptic actions. The first concerns postsynaptic neurotransmitter action. As summarized in Chapter 3, neurotransmission from hair cells to afferents involves the release of glutamate acting on AMPA receptors. Receptor activation occurs too fast (≈1 ms) to contribute to response dynamics (Dingledine et al. 1999). Processes having slower kinetics include receptor desensitization, clearance by transporters, and non-quantal transmission. These have only minimal effects on response dynamics, as is indicated by the fact that there is no consistent discrepancy between quantal phases (Fig. 4.14B) and depolarization phases (Fig. 4.14C).

The discrepancy between postsynaptic depolarization and spike discharge can be considered a form of postsynaptic adaptation. Traditionally, such adaptation was ascribed to continual spiking activity (Goldberg and Fernandez 1971a; Taglietti et al. 1977). To study this, sinusoidal galvanic currents were introduced via the perilymphatic space in mammals and were shown to

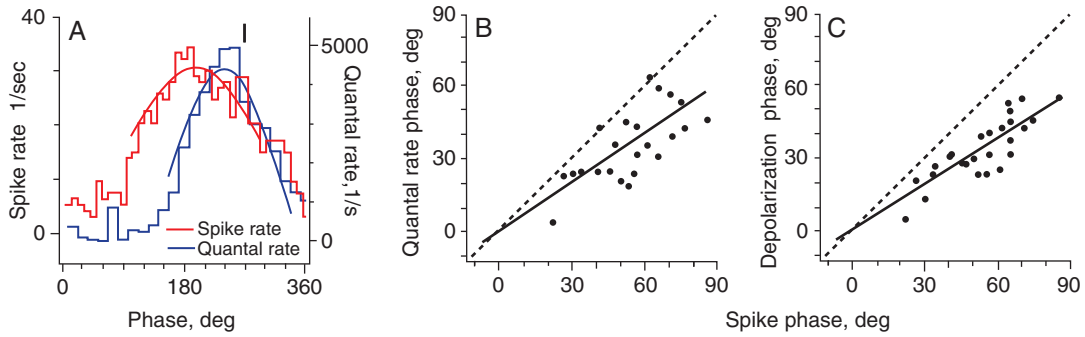

Figure 4.14 Comparing phases of quantal activity, postsynaptic depolarization, and spike activity for turtle posterior-crista units in response to a 0.3-Hz sinusoidal stimulus, an indentation of the posterior canal duct. Spike activity was collected before and synaptic activity after spikes were blocked by TTX. Approximately 30 degrees of the 60-degree variation in spike phase can be accounted for by quantal phase, which is interpreted as a presynaptic contribution; the remaining 30 degrees may be the result of postsynaptic factors. **A**. Phase histograms of spike activity (*left ordinate*) and of quantal rate (*right ordinate*) versus stimulus phase for an individual unit, turtle posterior crista. Peak excitatory stimulus, 270 degrees (*vertical bar*). Phase re stimulus of spike rate (63 degrees) leads that of quantal depolarization (48 degrees). **B**. Phases of quantal rate (*ordinate*) versus that of spike discharge (*abscissa*) for 23 units. *Dashed line*, unity diagonal. *Solid line*, best-fitting straight line. **C**. Phases of postsynaptic depolarization versus that of spike discharge, same 23 units. There is no significant difference between the two phase measures of synaptic activity, quantal rate (**B**) and postsynaptic depolarization (**C**). (Modified from Holt et al. 2006b)

directly activate the postsynaptic spike encoder (Ezure et al. 1983; Goldberg et al. 1982). The currents resulted in sinusoidal responses with phase leads of 10 to 15 degrees that were similar in all units. Because of the similarity, this form of adaptation could not contribute to afferent diversity. In the toadfish, some of the phase lead observed in irregularly discharging, phasic afferents could be blocked by GABA-B antagonists (Holstein et al. 2004b). This was related to the observation that some hair cells are GABAergic (Holstein et al.2004a). The mechanisms by means of which GABA might exert its presumed postsynaptic actions remains to be elucidated (Holt et al. 2006b).

Variations in Gain and Phase

Gain and phase vary with discharge regularity (Baird et al. 1988; Haque et al. 2004; Hullar et al. 2005; Ramachandran and Lisberger 2006; Sadeghi et al. 2007b). In Figure 4.15A,B, gain and phase for 2-Hz sinusoidal head rotations are plotted versus cv* for several extracellularly recorded units in the chinchilla. The gain plot provides evidence for two populations. Units in the first population range from very regular (cv* = .025 (to modestly irregular (cv* ≈ 0.25) and gain increases linearly with cv*. For the irregular units of the first group, gains approach 2 spikes s^{-1}/deg s^{-1}. The second population consists of the most irregular units in the sample; the gains of these afferents are about five times lower than would be predicted from an extrapolation of the regression line for the first group (Fig. 4.15A). Remarkably, there is only a single relation between phase and cv* for the units of the two populations (Fig. 4.15B). Phases range from lags of 5 to 10 degrees in the most regular units to leads near 30 degrees in the most irregular units. The presence of two groups, first established in the chinchilla (Baird et al. 1988; Hullar et al. 2005), was later confirmed in monkeys (Haque et al. 2004) and the mouse (Yang and Hullar 2007).

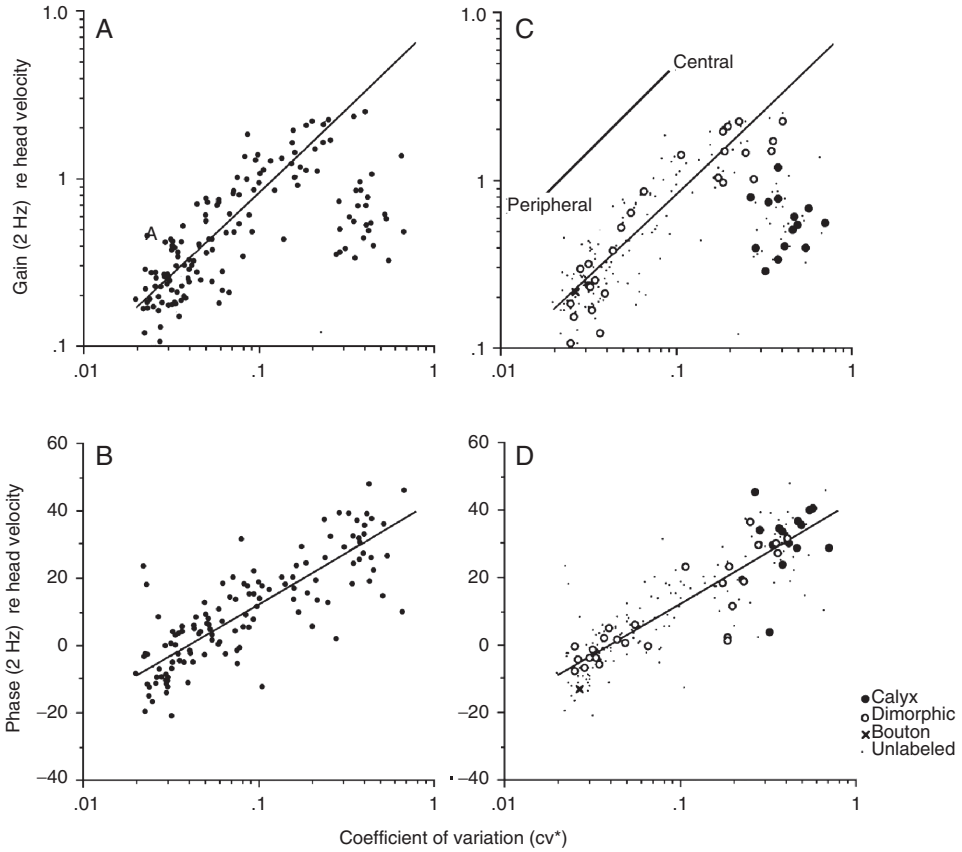

Figure 4.15 Gains and phases versus normalized coefficient of variation (cv*). Semicircular-canal afferents in the chinchilla responding to 2-Hz sinusoidal head rotations. Each point represents one unit. **A, B**. Extracellularly recorded units. Based on their gains, units fall into two groups. *Straight line* in **A** is best-fitting power law relation between gain and cv* for one of the groups. *Straight line* in **B** is best-fitting semilogarithmic relation between phase and cv* for all units. **C, D**. Corresponding data for intracellularly labeled units (see Key). Unlabeled units are shown as *small dots*. Labeled units: 14 calyx units, 26 dimorphic units, and one bouton unit. Calyx units are the most irregularly discharging afferents and have the largest phase leads and distinctively low gains. Gain and phase of dimorphic units increase with cv*; regular units are found in the peripheral zone and irregular units in the central zone. The one bouton unit was regular, had a low gain and phase, and was located in the peripheral zone. Gains, spikes•s^{-1}/deg•s^{-1}; phases in degrees re head velocity with positive values indicating phase leads. (From Baird et al. 1988)

Two factors contribute to the gain versus cv* relation for the first group. By far the more important of these is the sensitivity of the post-synaptic spike encoder, which can be measured by the galvanic sensitivity of individual afferents (Goldberg et al. 1984; Smith and Goldberg 1986). The other factor is the high-frequency gain enhancement associated with the more phasic response dynamics of irregular units. When the influence of response dynamics is eliminated, the gain curve of the first group parallels the relation between galvanic sensitivity and cv* (see Fig. 4.4B). Since galvanic sensitivity provides a measure of encoder gain, the parallel between the two relations implies that the synaptic input to the encoder is nearly constant for

units of the first group. By the same reasoning, since their galvanic sensitivity is in line with their discharge regularity, synaptic input is about 5x lower for units of the second group.

Afferent Morphology and Physiology

The first attempt to relate afferent diversity with morphology compared physiological estimates of fiber size with discharge regularity and other discharge properties (Goldberg and Fernández 1977; Lysakowski et al. 1995; Yagi et al. 1977). A more direct approach, done in the chinchilla, involves the intra-axonal labeling of physiologically characterized fibers (Baird et al. 1988). With this method, fibers are impaled and their physiology is characterized, after which a label is iontophoresed from the recording microelectrode and travels down the axon to its peripheral terminations. Similar studies have been done in non-mammalian vertebrates (Boyle et al. 1991; Brichta and Goldberg 2000a; Myers and Lewis 1990; reviewed in Lysakowski and Goldberg 2004).

The results of intracellular labeling in the chinchilla are summarized in Figure 4.15C,D. Unlabeled (small symbols) and labeled fibers (large symbols) are included in the figure. As expected from extracellular labeling studies (see Fig. 2.14), intracellularly labeled calyx units were found to terminate in the central zone. These fibers are irregularly discharging units with relatively small gains and large phase leads (λ). In short, calyx units are the second group of irregularly discharging units identified in extracellular recordings. Dimorphic units belong to the first group (μ). The physiology of dimorphic units depends on their locations in the crista. Those terminating in the central zone are irregularly discharging with large gains and phases. In addition to their lower gains, calyx units are slightly more irregular in their discharge and have slightly larger phases than central dimorphs. Peripheral dimorphs are regularly discharging and have small gains and phases.

Only one intra-axonally labeled bouton unit could be traced to its neuroepithelial termination in the peripheral zone. Like peripheral dimorphic units, the bouton unit was regularly discharging and had small gains and phases. The paucity of labeled bouton fibers presumably reflects their small axon diameter, which makes them difficult to impale. Fortunately, their small diameter also makes it possible to identify bouton units in extracellular recordings by their small conduction velocities. This was done in the squirrel monkey (Lysakowski et al. 1995). As might be expected, the presumed bouton units are regularly discharging with small gains and near-zero phases.

The results, particularly those for dimorphic units, emphasize the importance of regional variations in discharge properties. Within this single morphological class, there is an almost 10-fold variation in rotational gain between afferents innervating the peripheral and central zones, a comparable variation in encoder (galvanic) sensitivity, and a large variation in response dynamics as judged by a 30- to 40-degree difference in the 2-Hz rotational phases of afferents innervating the two zones. Reinforcing the importance of regional variation are the similarities in discharge properties between peripheral dimorphic and bouton units and between central dimorphic and calyx fibers.

Of the various differences in afferent discharge, only the large discrepancies in rotational gains of calyx fibers and their central dimorphic neighbors do not reflect regional variations. It should be emphasized that the lower sensitivity of calyx fibers is unrelated to their encoder sensitivity. In fact, calyx units have the most irregular discharge, the largest phase leads, and the largest galvanic responses of the entire population. Their relatively large phase leads suggest that the rotational gains of calyx units should increase with frequency faster than those of irregular dimorphic units. This is the case at least in the chinchilla. As frequency increases towards 10 Hz, the gains of calyx units approach those of irregular dimorphs (Hullar et al. 2005). On the other hand, gain versus frequency curves for calyx and high-gain irregular units in the monkey parallel one another (Ramachandran and Lisberger 2006; Sadeghi et al. 2007b).

The higher synaptic gains of dimorphic as compared to calyx units might be explained by the auxiliary inputs the former receive from type II hair cells. A scheme in which type I and type II inputs sum linearly leads to an estimate that

each type I hair cell contributes three times the synaptic input to an afferent than it receives from each of its bouton contacts (Baird et al. 1988). A 3:1 ratio is less than the 10:1 ratio in the number of ribbon synapses made with individual calyx and bouton endings (Lysakowski and Goldberg 1997). The discrepancy in these ratios may be related to the distinctive features of synaptic transmission between type I hair cells and their calyx endings. As reviewed in a previous chapter (Section 3.5, Synaptic transmission involving type I hair cells), synaptic transmission may be less efficient at calyx than at bouston endings. Another possibility is that synaptic transmission involving calyx endings may differ for the two afferent groups.

Dynamic Range of Afferent Discharge

In a preceding section (see Fig. 4.10), we saw that afferent responses behaved linearly at least for moderate angular head velocities. But response should eventually reach an upper limit. The question arises as to the value of the upper limit and the head velocities at which such saturating nonlinearities become evident. Excitatory responses as a function of head velocity are shown for three groups of afferents in Figure 4.16 (Plotnik et al. 1999). Relations between excitatory response (r) and head velocity (v) can be fit by the empirical function

$$r(v) = \frac{r_{MAX} v}{v_{1/2} + v} \qquad (4.8)$$

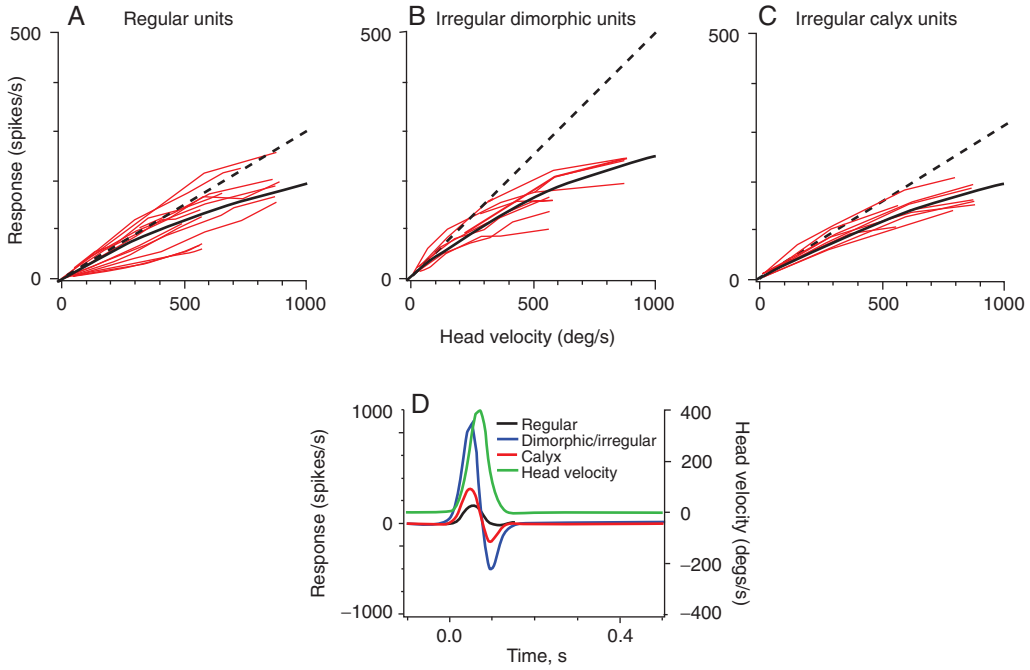

Figure 4.16 Relations between response and angular head velocity for three populations of semicircular-canal afferents in the chinchilla. Responses and head velocities, average values during last 0.5 s of a 2-s period of constant angular acceleration. For each population, a non-linear function (*solid line*, Equation 4.11) based on the average parameters for the population is compared with the corresponding linear function (*dashed line*). Regular units, cv* < 0.05 (**A**); non-calyx units, cv* > 0.20 (**B**); calyx units (**C**). Distinction between calyx and non-calyx units based on a quadratic discriminant function. **D**. Calculations of the responses in the squirrel monkey to a head saccade, peak velocity of 400 deg/s and peak acceleration of 10,000 deg/s^2. In the calculation we used the mean velocity and acceleration sensitivities from Lysakowski et al. (1995). (Data in **A–C** from Plotnik et al. 1999)

which is recognized as the Michaelis-Menten equation of enzyme kinetics. Here r_{MAX} is the maximum response and $v_{1/2}$ is a constant. For $v << v_{1/2}$, response is linear with a gain or slope of $r_{MAX}/v_{1/2}$. As velocity increases beyond $v_{1/2}$, response approaches an asymptote, r_{MAX}. For all units, r_{MAX} is 300 to 500 spikes/s (Plotnik et al. 1999).

Is this r_{MAX} adequate to handle the head rotations encountered in everyday life? The angular velocities obtaining during locomotor activities seldom exceed 200 deg/s (Grossman et al. 1988). Even rapid voluntary head movements are rarely larger than 400 deg/s, although accelerations can be near 10,000 deg/s^2 (Armand and Minor 2001; Liao et al. 2005). In Figure 4.16D, we have calculated the response to a 400 deg/s head saccade assuming linear rate-intensity relations. The peak response of calyx units (300 spikes/s) is close to r_{MAX}, while that of irregular dimorphs (1,100 spikes/s) clearly exceeds this limit.

These calculations suggest that the low gains of calyx units allow them to encode rapid head movements without reaching excitatory saturation. But a low gain cannot be the entire story since regular units have even lower gains and smaller peak responses. This suggests that the distinctive function of calyx units involves the combination of its ability to handle fast head movements and the other properties that distinguish irregularly discharging units. Of the other properties, phasic response dynamics would seem most relevant since they allow the peak responses of calyx and other irregular afferents to anticipate peak head velocity and, thus, could compensate for delays in various reflex pathways (Huterer and Cullen 2002; Minor et al. 1999; Ramachandran and Lisberger 2005).

Type I hair cells and calyx endings are a recent evolutionary feature, being seen only in reptiles, birds, and mammals (Lysakowski 1996; Wersäll 1956). These animals are distinguished from their aquatic and amphibian ancestors in having mobile necks, allowing for head movements on a nearly stationary body. It can be supposed that the low-gain calyx afferents, seen in turtles as well as mammals, were an adaptation allowing the semicircular canals to accommodate the rapid rotations made possible by the freeing of head movements from the rest of the body. This kind of reasoning raises an intriguing question. If, as suggested, the role of these afferents is related to their relatively low rotational gains and phasic response dynamics, it is unclear why these discharge properties would require the elaborate structure of the calyx ending.

4.3 OTOLITH ORGANS

Afferents innervating otolith organs respond to linear but not to rotational forces acting on the head (Goldberg and Fernandez 1975). Linear forces arise when the head is accelerated along straight lines. Because of the presence of gravity, afferents also signal head tilts with respect to the earth vertical. In fact, because the otolith organs are linear-force sensors, their response should be indistinguishable for a head tilt and a linear acceleration of appropriate magnitude and direction (Angelaki et al. 2004; Fernández and Goldberg 1976b).

Directional Properties

The responses of otolith afferents depend on the orientation of linear forces with respect to the head. Directional properties for each fiber can be summarized by a unit polarization vector, $\mathbf{v} = (x, y, z)$, expressed in head-fixed coordinates (see Fig. 1.1)[1] and reflecting the polarization vectors of the innervated hair cells (Angelaki and Dickman 2000; Fernández et al. 1972; Loe et al. 1973; Tomko et al. 1981a). The directional properties of peripheral otolith neurons can be termed one-dimensional (1D) as they can be characterized by a single vector. In contrast, many central otolith neurons have two-dimensional (2D) tuning summarized by a response ellipse (Angelaki et al. 1993; Angelaki and Dickman 2000; Bush et al. 1993). Two-dimensional tuning can result from the convergence of otolith inputs differing in both their spatial and temporal properties (Angelaki 1992) (see Chapter 7).

1. The coordinate system illustrated in Figure 1.1 has been generally adopted in the literature and is used here. Some studies of otolith afferent discharge (Fernandez et al. 1972; Fernández and Goldberg 1976a–c; Loe et al. 1973) used a different system. We have transformed the data to be consistent with Figure 1.1.

The 1D spatial tuning of peripheral otolith neurons is illustrated by the response of a utricular unit to pitch and roll head tilts (Fig. 4.17A). As the head is tilted to various positions, there is a sinusoidal modulation of discharge rate about an average or zero-force discharge (d_0). A sinusoidal modulation implies that the response for any tilt position is proportional to the component of the polarization vector coincident with the gravity vector. To see this, we use matrix algebra, specifically a rotation matrix, to transform the gravity vector, $\mathbf{g} = (0,0,-1)$ in earth-fixed coordinates, to $\hat{\mathbf{g}} = (\sin P, \sin R \cos P, -\cos R \cos P)$ in head-fixed coordinates; R is the roll angle and P is the pitch angle. The force (F) acting on otolith receptors is calculated as the scalar product (F) of the transformed gravity vector $(\hat{g})$ and a head-fixed polarization vector, $(\boldsymbol{v} = \boldsymbol{x,y,z})$, i.e.,

$$F = v \bullet \hat{g}$$
$$= x \sin P + y \sin R \cos P - z \cos R \cos P \quad (4.9)$$

Presumably, $\boldsymbol{v}$ reflects the morphological polarization of the hair cells innervated by the afferent. We tentatively assume that the discharge, $d(R,P) = sF + d_0$, is a linear function of F. The sensitivity factor (s in spikes/s•g) converts F to a discharge rate. d_0 is a resting (zero-force) discharge. Here and elsewhere, g is the acceleration of gravity, 980 cm/s^2. Equation 4.9 becomes

$$F = y \sin R - z \cos R \quad (4.9a)$$

for pure rolls (P = 0) and

$$F = x \sin P - z \cos P \quad (4.9b)$$

for pure pitches (R = 0). Since F and $d(R, P)$ are sinusoidal functions of tilt angle for pure rolls or pure pitches, a Fourier analysis can be used to extract the coordinates of $\mathbf{V} = s\boldsymbol{v} = (X, Y, Z)$. Sensitivity ($s$), the response obtained when the polarization and gravity vectors coincide, is estimated from the length of $\mathbf{V}$, (i.e., $s = \sqrt{X^2 + Y^2 + Z^2}$). The normalized polarization vector, $\boldsymbol{v} = \mathbf{V}/s$, summarizes directional properties. To calculate d_0, we take the discharge rate obtained when the transformed gravity vector, $\hat{\mathbf{g}}$, is orthogonal to $\boldsymbol{v}$ (i.e., $F = 0$). The condition is met at two points during pitches, rolls, or any other tilt series around a great circle. The two points are recognized as being 180 degrees apart, yet having the same discharge rate. For the unit illustrated in Figure 4.17, s = 28 spikes/s•g and d_0 = 40 spikes/s. $\boldsymbol{v}$ = (0.707, 0.707,0.035) is halfway between the vectors pointing out the nose and out the ipsilateral (left) ear. Its small z component implies that $\boldsymbol{v}$ lies close to the horizontal plane, which is taken as the plane of the horizontal semicircular canal.

The assumption that response $(d–d_0)$ is linearly related to effective force (F) is examined in Figure 4.17B, C. It is seen that the relation is nonlinear with excitatory responses being larger than inhibitory responses. The nonlinearity becomes more obvious when centrifugal forces of more than 1 g are introduced (Fig. 4.17B). Remarkably, points for centrifugal forces (③) and static tilts (④) overlap even though they represent different physical circumstances. As noted previously, the equivalence between gravity and a linear acceleration is to be expected of a linear-force sensor. To handle the nonlinearity we calculate F by linear algebra (Equation 4.9) and consider the response to be a nonlinear function of F. In the particular case of Figure 4.16C, response can be fit by the second-order polynomial, $d - d_0 = s(F + \alpha F^2)$ with s = 32.5 spikes/s•g and α = 0.41. The use of a quadratic nonlinearity holds only for forces in the range ±1 g. A more adequate formulation is presented later (Fig. 4.24).

A vector depiction of directional properties requires that forces orthogonal to a unit's polarization vector should be ineffective. Tests of this prediction are shown in Figure 4.18 for a unit whose polarization vector lies near the horizontal plane of the utricular macula. Centrifugal forces were used to determine the effects of orthogonal forces. Two kinds of orthogonal forces have to be considered: *compressional* forces directed perpendicular to the macular plane and *shearing* forces in the macular plane. Compressional forces are ineffective. Not only do they not lead to a response (Fig. 4.18C), but they also do not influence responses to simultaneously applied shearing forces (Fig. 4.18E). Contrary to predictions, orthogonal shearing forces lead to excitatory responses (Fig. 4.18B). When response is plotted versus force direction, excitatory responses are produced by shearing forces spanning 225 degrees, not the expected 180 degrees (Fig. 4.18D). The last result is inconsistent with a vector treatment of directional selectivity.

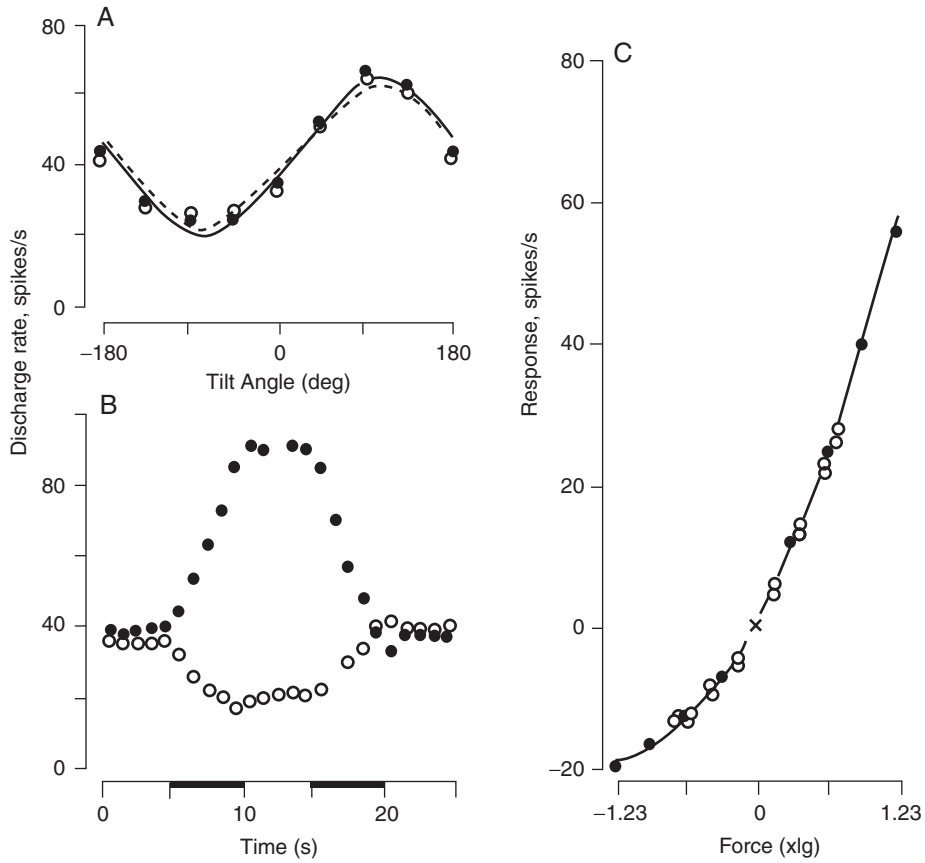

Figure 4.17 Responses of an otolith afferent to static tilts and to centrifugal forces. **A**. Responses to static rolls (③ ③) and pitches (④ ④). Lines are best sinusoidal fits to roll (—) and pitch (**---**) responses. Maximum excitatory responses, ipsilateral rolls and forward pitches. **B**. Responses to centrifugal forces, parallel (excitatory, ③) and anti-parallel (inhibitory, ④) to polarization vector, the latter determined by static tilts in **A**. Plateau force, 1.23 g. Excitatory response is larger than inhibitory response. **C**. Comparing responses to static tilts and centrifugal force. Non-linear relation between response and force is the same for centrifugal forces (③) and static tilts (④). Fit is a quadratic polynomial. (From Fernández and Goldberg 1976a)

Three comments can be made. First, the effect cannot be explained by a convergence of hair-cell inputs differing in their direction properties (Fernández et al. 1972). Second, the orthogonal-shear effect is sufficiently small that a vector treatment still provides a useful approximation. Third, the effect is consistent with micromechanics. Only the kinocilium and possibly the tallest stereocilia are directly attached to the otoconial membrane (Kachar et al. 1990; Lim 1984). This being the case, an orthogonal shear will be communicated to the remainder of the hair bundle by the stretching of filamentous strands, including tip links, connecting the kinocilium and stereocilia in adjacent ranks. The result should be a fanning of the hair bundle and an opening of transducer channels for either direction of orthogonal shear. As expected from hair-bundle geometry, responses during orthogonal shears are smaller than those produced by shears parallel to the polarization vector. Inhomogeneities in the overlying otoconial membrane have been proposed as contributing to orthogonal shear responses (Kondrachuk 2002).

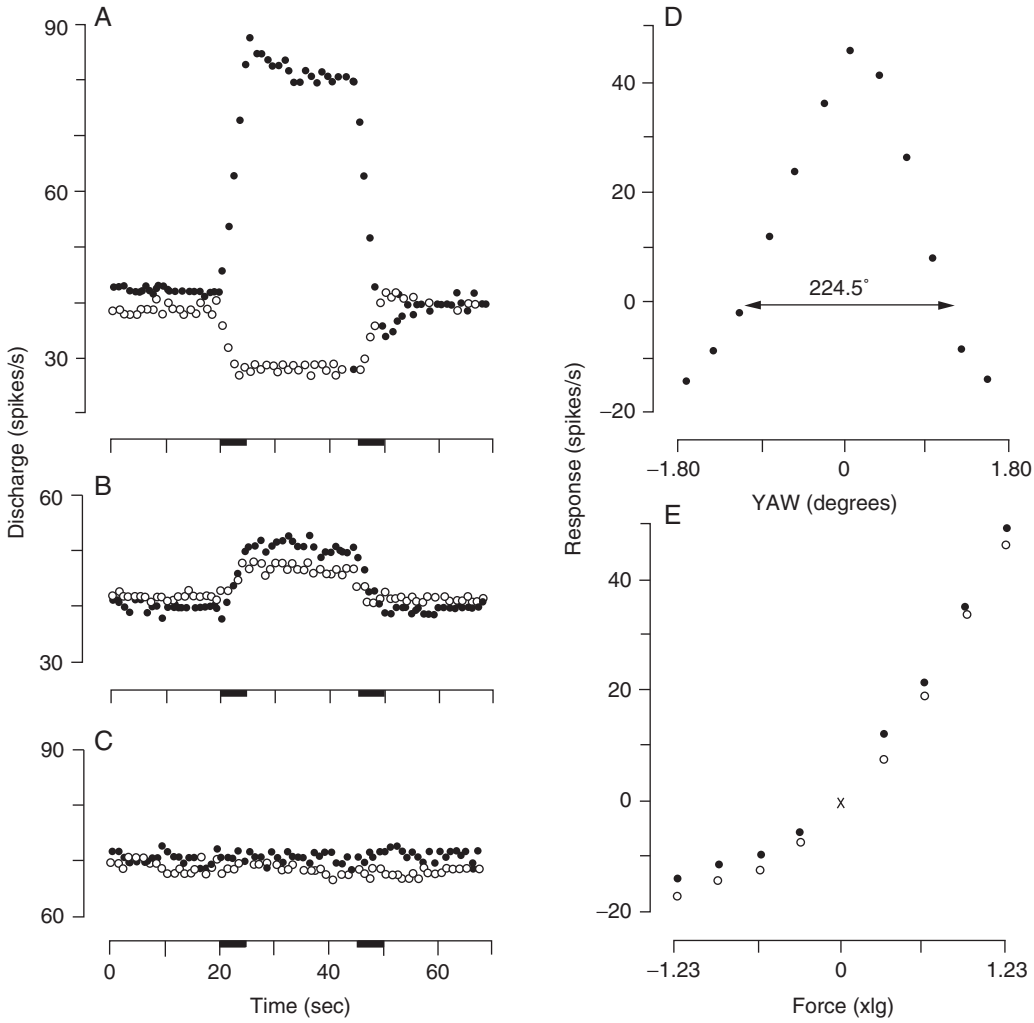

Figure 4.18 Comparison of responses to shearing and compressional forces for a utricular afferent i. Polarization vector pointed out the nose. Responses are to centrifugal-force trapezoids, 1.23 g peak force. **A**. Responses to shears parallel (excitatory, ③) and anti-parallel (inhibitory,④) to the unit's polarization axis. **B**. Shears orthogonal to polarization axis, force through ipsilateral (③) and contralateral (④) ears, lead to excitatory responses, ≈25% of maximal excitatory response to parallel shears. **C**. There are no responses when the forces are orthogonal compressions exerting pressure (③) or traction (④) on the macula. **D**. Response versus angle between polarization and shear force vectors. Excitation is seen for angles subtending 225 degrees. **E**. Responses to parallel shears of varying magnitude when gravity exerts pressure (③) or traction (④) on the macula. Not only do compressional forces not lead to responses, they also do not alter the responses to simultaneous shearing forces. (From Fernández and Goldberg 1976b)

Otolith afferents are sensitive to shearing forces, but not to compressional forces. This finding has implications for the complementary functions of the utricular and saccular maculae (Fernández and Goldberg 1976a; Tomko et al. 1981a). The main part of the utricular macula lies in a horizontal plane, while its anterior part curves upward. Utricular afferents, at least those from its main part, should have horizontally disposed polarization vectors (see Figs. 2.5 and 2.6). Responses to

static tilts are shown in Figure 4.19A–H for eight units independently assigned to the superior vestibular nerve (SN). We suppose that such units arise from the utricular macula, although some of them may supply the anterior part of the saccular macula (see Fig. 2.2). For all eight units, there is little difference in discharge rates for prone (0 degrees) and supine (180 degrees) positions, consistent with their polarization vectors having relatively small z components and, thus, lying near the horizontal plane. Some units are excited by ipsilateral rolls (Fig. 4.19A–E), others by contralateral rolls (Fig. 4.19F–H), some by downward pitches (Fig. 4.19D,E H), and others by upward pitches (Fig. 4.19A,B,F). Some units respond almost equally to pitches and rolls (Fig. 4.19B,D,F), others predominantly to rolls (Fig. 4.19C,G). Stated in terms of vector coordinates, there are units with various combinations of ±x and ±y coordinates. This diversity is consistent with the fanlike disposition of morphological polarization vectors in the utricular macula (Fig. 4.20, left bottom). In fact, each of the units can be assigned an approximate macular location based on its vector components (Fig. 4.19L). Neither the sensitivity (s) nor the resting discharge (d_0) is correlated with the directional properties of utricular afferents. Typical values are 40 to 90 spikes/s for d_0 and 20 to 50 spikes•s^{-1}/g for s. In only a few units and none in Figure 4.19 is discharge abolished at any tilt angle.

Quite different directional properties are seen in units recorded from the inferior vestibular nerve (IN), which innervates the main part of the saccular macula (Fernández et al. 1972; Fernández and Goldberg 1976a; Tomko et al. 1981a) (see Fig. 2.2). Such units usually have polarization vectors with large z components (Fig. 4.19I). Based on the sign of the component, saccular units have maximum rates near the supine (+z) or prone (–z) positions. From the polarization map (Fig. 4.20, right bottom), the units should be located dorsal (+z) or ventral (–z) to the striolar dividing line. As is illustrated in Figure 4.19I, saccular units with +z and –z components differ considerably in their resting values. Higher values of d_0 are found in +z units than in –z units. Sensitivities are slightly higher for +z units. One result of these differences is that the discharge rates of +z and –z units are much closer in the prone (0 degrees) than in the supine (180 degrees) positions. Once again, discharge is seldom abolished in any head position.

One way to appreciate the difference in directional properties for the two populations is to compare the angles their polarization vectors make with the horizontal (utricular) plane. Angles are less than 30 degrees for most utricular afferents and more than 60 degrees for most saccular afferents (Fig. 4.19J). Another way is to plot normalized vectors for the two maculae in spherical coordinates. The utricular vectors are best viewed from the +z axis, where they are seen to be within 30 degrees of the horizontal plane (Fig. 4.20, left, outer ring). There is a preponderance of +y vectors, but otherwise the vectors are widely distributed within this ring. Saccular vectors are best viewed from the ipsilateral ear, where they are seen to align near the vertical axis (Fig. 4.20, right). The results are consistent with the conclusion that the utricular macula provides a broad, two-dimensional representation of linear forces acting in the horizontal plane, while the saccular macula adds the third or vertical dimension. During locomotion and many other everyday activities, vertical linear accelerations are much larger than their horizontal counterparts (MacDougall and Moore 2005; Pozzo et al. 1990), indicating the importance of the saccular macula during these behaviors. Utricular afferents are most sensitive to small tilts from upright, suggesting that the latter organ may be especially involved in the maintenance of an upright posture.

In the squirrel monkey, utricular units excited by ipsilateral roll tilts outnumber those excited by contralateral roll tilts by a 3:1 ratio (Fernández et al. 1972; Fernández and Goldberg 1976a). A similar preponderance of ipsilaterally excited utricular units was observed in the cat (Loe et al. 1973). In contrast, in the chinchilla, ipsilaterally excited utricular units were only in a slight majority (Goldberg et al. 1990a). The ratios based on tilt responses can be compared to the ratio of utricular areas whose polarization vectors point laterally and medially. In both the squirrel monkey and chinchilla, the proportion of ipsilaterally excited units is slightly larger than would be predicted on an areal basis. For the monkey saccular macula, there were approximately equal numbers of units with +z and –z components

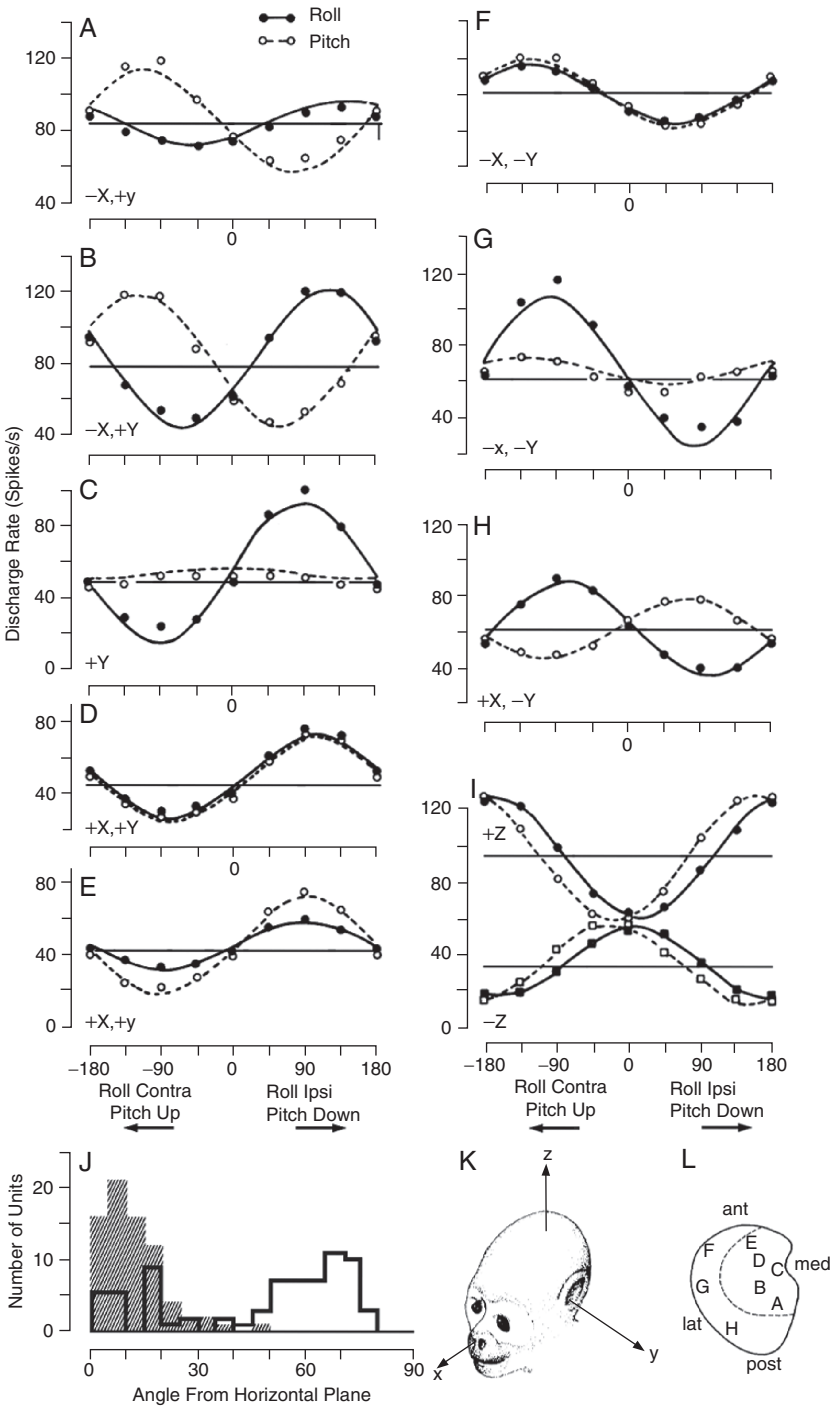

Figure 4.19 Discharge rate from several otolith afferents in the squirrel monkey are plotted as functions of tilt angle about pitch and roll axes. **A–H**. Each graph represents data from one unit recorded from the superior vestibular nerve (SN) and presumably innervating the utricular macula. **I**. Two units recorded from the inferior vestibular nerve (IN) and presumably innervating the saccular macula. **J**. Static-tilt data, such as shown in **A–I**, were used to calculate a polarization vector for each unit. Vectors for SN (*gray-filled bars*) and IN units (*unfilled bars*) differ in the angle they make with the horizontal plane. SN vectors lie near the horizontal (utricular) plane, while IN units lie near the vertical (saccular) axis. **K**. Locations of utricular afferents (**A–H**) inferred by comparing polarization vectors calculated from tilt data with morphological-polarization maps (see Fig. 2.9). (From Fernández and Goldberg 1976a)

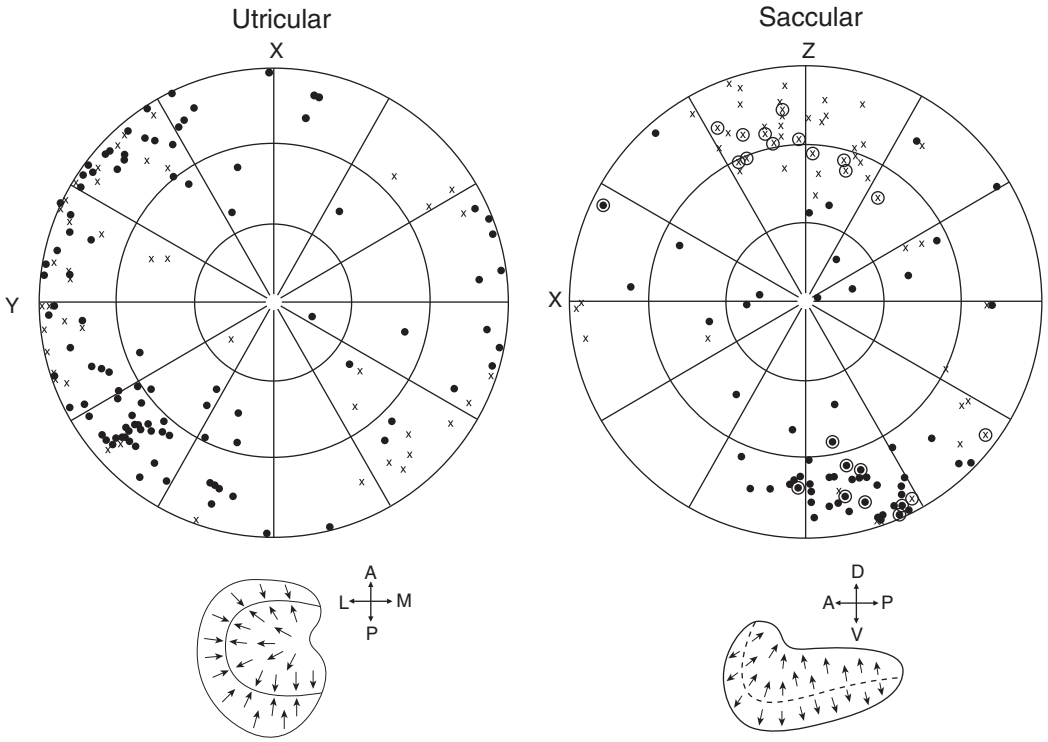

Figure 4.20 Distribution of polarization vectors, otolith afferents, squirrel monkey. Each point represents the polarization vector for a single unit in spherical coordinates. Units were assigned to the utricular or saccular maculae based on the semicircular-canal units encountered in the same puncture. λ and x, vectors pointing, respectively, towards and away from the reader. *Left:* Utricular vectors are best viewed from the top of the head. The further a point is from the z pole, the larger is the horizontal component of its vector. Most points for utricular vectors lie in the outer ring, signifying large horizontal components. *Right:* Saccular vectors are best viewed from the ipsilateral (left) ear. Most saccular vectors have large z components and lie along an axis slightly tipped with respect to the vertical. The circled points were obtained from the inferior vestibular nerve after section of the superior vestibular nerve. Below each spherical plot is the polarization map for the corresponding macula. Directions: *A*, anterior; *P*, posterior; *M*, medial; *L*, lateral; *D*, dorsal; *V*, ventral. Coordinates follow the same convention as in Figure 4.19K. (From Fernández and Goldberg 1976a)

(Fernández and Goldberg 1976a). This is so despite the fact that the area dorsal to the striola is considerably larger in the monkey than its ventral counterpart (Lysakowski and Goldberg 2008).

Macromechanics and the Otoconial Membrane

The otolithic or otoconial membrane (OM) is a flattened gelatinous structure, approximately 60 μm high, covering the underlying neuroepithelium of the utricular or saccular macula and made up of three layers (Fig. 4.21) (Kachar et al. 2000; Lim, 1984). Calcium carbonate crystals are embedded in the otoconial layer (OL), a loose fibrous network at the top of the membrane (Fig. 4.21A,B). In mammals the crystals are in the form of calcite (Carlström 1963; Ross and Pote 1984) and are formed around organic matrices. In each otolith organ, the crystals have a characteristic pattern (see Fig. 2.7), which is

laid down during development. Because the crystals are denser than the surrounding endolymph, the otoconial layer is displaced when acted on by linear forces such as occur in a gravitational field or when the head is accelerated in a straight line. Much remains to be learned about the otoconia, including their initial formation, the cues responsible for their elaborate patterning in each organ, and their maintenance during life (Lundberg et al. 2006; Thalmann et al. 2001; Zhao et al. 2007).

Lying underneath the OL is the gelatinous layer (GL), a relatively rigid structure consisting of a dense, randomly oriented, cross-linked filamentous network (Fig. 4.21D) that couples motion of the OL to underlying structures. The lowest or columnar layer (CL) (Fig. 4.21C) is a looser meshwork of vertically arranged filaments, anchored to the apical surfaces of supporting cells and sometimes referred to as the subcupular meshwork (Dohlman 1971; Lim 1984). Given its anisotropic structure, the CL is likely to be the most compliant of the three layers in shear.

We consider the influence of otoconial membrane structure on response dynamics and directional properties, beginning with the latter topic and concentrating on the insensitivity of the maculae to compressional forces. The OM contains glycoproteins and proteoglycans (Goodyear and Richardson 2002) and can be described as a fibrous network embedded in a hydrated gel. In addition, hair bundles are sequestered in clearings or tunnels in the CL (Fig. 4.21, middle) (Kachar et al. 1990; Lim 1984; but see Ross et al. 1987). These structural features can explain the insensitivity of the otolith organs to non-shearing forces. Because hydrated gels have a turgor pressure, they can resist compression (Alberts et al. 2002). At the same time, the fibrous network of the CL should attenuate the effects of traction.

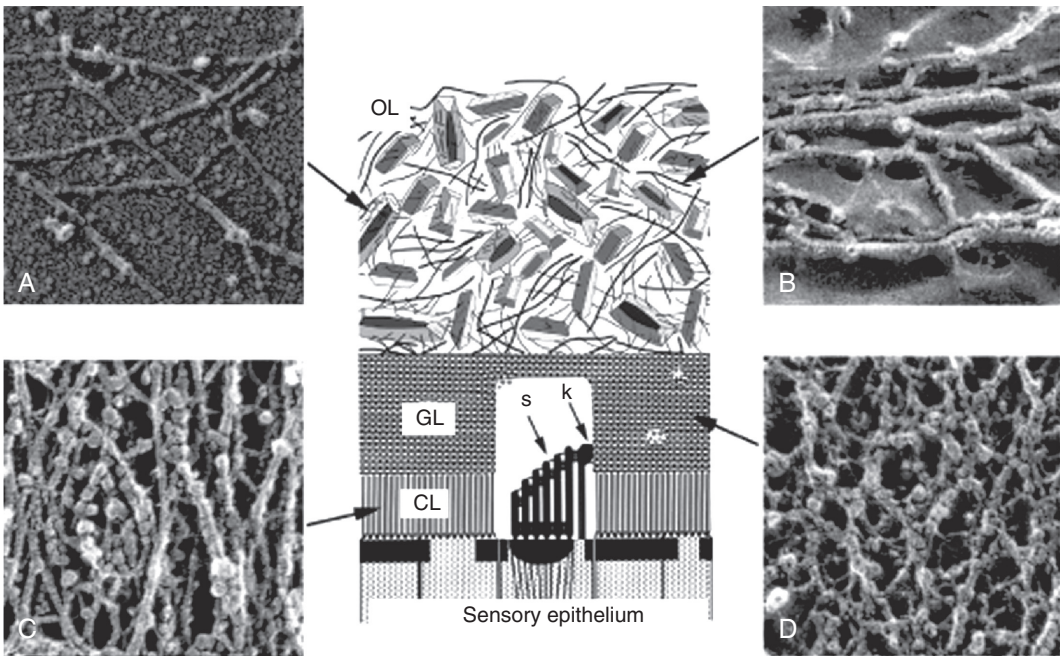

Figure 4.21 The otoconial membrane (OM) is composed of three layers. *Middle*: Schematic of the three layers: *OL*, otoconial layer; *GL*, gelatinous layer; *CL*, columnar layer. Shearing displacements of the CL are communicated to the stereocilia (*S*) by way of the kinocilium (*K*). **A–D**. Freeze-etch specimens of the three layers. **A**, **B**. The OL consists of $CaCO_3$ crystals embedded in a loose meshwork. Only the meshwork is seen here. **C**. In the CL, the fibers are oriented so as to be compliant to shearing, but not to compressional, forces. **D**. The GL consists of a dense meshwork of randomly oriented fibers that give it rigidity in all directions. (From Kachar et al. 1990)

Sequestering the hair bundles in fluid compartments should contribute to their shielding from compressional forces.

Turning to response dynamics, both direct observations of otoconial motion (de Vries 1950) and afferent recordings (Angelaki and Dickman 2000; Fernández and Goldberg 1976c) indicate that the mechanics are overdamped. To prevent underdamped oscillations requires much more damping than can be provided by the viscous drag exerted by the endolymph (Grant and Best 1986), suggesting that the OM itself provides the necessary damping by being viscoelastic (i.e., combining the properties of a viscous fluid and an elastic solid). This is the expected mechanical behavior of a hydrated gel. A one-dimensional model incorporating this idea has been developed (Grant and Cotton 1990; Grant et al. 1994; Kondrachuk 2001b, 2002). The model includes two simplifications: (1) the OM is considered as lying in a single plane and (2) the GL and CL are considered as a single layer, which is referred to as the GL. Once the basic equations are evaluated, we can consider the influence of the two simplifications. (Kondrachuk 2001b),

Our treatment follows that of Kondrachuk (2001b) beginning with the second-order partial differential equation,

$$\Delta\rho\frac{\partial^2 X}{\partial t^2}+\mu\frac{\partial^3 X}{\partial t\partial Z^2}+\frac{E}{2(1+\sigma)}\frac{\partial^2 X}{\partial Z^2} = \Delta\rho\bullet A_X(t) \quad (4.10)$$

X is the shearing displacement of the GL and Z its height measured from the surface of the neuroepithelium. Otoconial displacement is the result of a difference in density, $\Delta\rho=\rho_{OL}-\rho_{ENDO}$, between the OL and the surrounding endolymph. $A_X(t)=g_X(t)-a_X(t)$ is referred to as the gravitoinertial force (GIF) and is the sum of the gravitational force [$g_X(t)$] and the oppositely directed linear acceleration [$-a_X(t)$] acting in the X or shearing direction. The left side of equation 4.10 consists of an inertial term and two restoring terms, one related to the GL's viscosity and the other to its elasticity. The GL is characterized by a coefficient of viscosity (μ), an elastic (Young's) modulus (E), and a Poisson's ratio (σ). The model is one-dimensional as the macula does not respond to compressional forces (Fernández and Goldberg 1976b; Kondrachuk 2001a) and the lateral extent of the macula is so much larger than the thickness of the OM that edge effects can be ignored. The viscous drag exerted on the top surface of the OL by the endolymph is neglected because it is much too small to result in overdamped dynamics.

To evaluate Equation 4.10 requires a value for $\Delta\rho$. We will use $\Delta\rho$ = 0.33 gm/cm^3, a value measured by Steinhausen (1935). A higher value of $\Delta\rho$ was reported by Trincker (1962). Setting σ = 0.5 makes the GL incompressible. One approach to estimating E is to consider steady-state displacements by setting the time derivatives in Equation 4.10 to zero and $A_X(t)$ to $\overline{A_X}$, a constant linear force. The result is

$$\frac{\partial^2 X}{\partial Z^2}=\frac{2\Delta\rho\overline{A}_X(1+\sigma)}{E} \quad (4.11)$$

with boundary conditions $X = 0$ at the neuroepithelial surface ($Z = 0$) and $\partial X/\partial Z = 0$ at the top of the GL ($Z = h$). E can then be evaluated after a double integration of Equation 4.11 to yield

$$E=\frac{(1+\sigma)\overline{A}_X\bullet\Delta\rho\bullet h^2[2(Z/h)-(Z/h)^2]}{X(Z)} \quad (4.12)$$

Studies of solitary hair cells suggest that maximal transduction occurs when hair bundles of 10 μm height are deflected in the excitatory direction by 1 μm—that is, X(Z = 10 μm) = 1 μm (Holt et al. 1997). From afferent recordings (Fernández and Goldberg 1976b), discharge in the excitatory direction typically saturates for linear forces near $\overline{A}=4g$ (see Fig. 4.25). Substituting these values into Equation 4.12 provides an E = 100 dyne/cm^2.

Because Equation 4.10 is second-order in its time derivatives, it is governed by two time constants, $\tau_1=2\mu(1+\sigma)/E$ and $\tau_2=\Delta\rho h^2/\mu$. An estimate of μ is provided by afferent-nerve recordings, which suggest that the response dynamics of the otolithic membrane are heavily damped with a lower corner frequency near 5 Hz, corresponding to a time constant, $\tau_1\approx$ 30 ms. With E = 100 dyne/cm^2, this value of τ_1 gives a value, μ = 1 poise, about 100 times the viscosity of water (or endolymph). The system is heavily damped because $\tau_2\approx 3\times10^{-3}$ ms, much smaller than τ_1.τ_2 is so small, in fact, that the OM should behave as a first-order system up to very high frequencies (>1,000 Hz) with response being

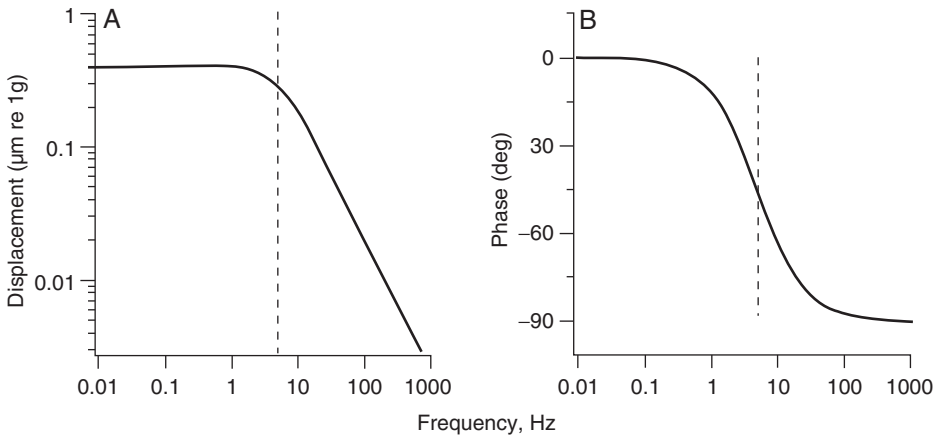

Figure 4.22 Bode plot, viscoelastic model of otoconial membrane, including gain (**A**) and phase (**B**) re gravitoinertial force. Lower corner frequency, 5 Hz. Upper corner frequency, >>1000 Hz. *Vertical dashed line* divides the spectrum in low- and mid-frequency regions in which the output parallels sinusoidal force (acceleration) and its integral (velocity), respectively.

proportional to linear acceleration up to 5 Hz and to linear velocity at higher frequencies (Fig. 4.22).

While the treatment is likely to be qualitatively correct, its quantitative properties must be viewed cautiously. For one thing, the estimate of τ_1 was obtained by assuming that the response dynamics of regular afferents are determined solely by OM macromechanics. As afferent response dynamics may include phase leads introduced by transduction mechanisms subsequent to OM displacement, $\tau_1$could be underestimated. Furthermore, the response dynamics were observed only up to 2 Hz; a study of higher frequencies might be revealing. Even more valuable would be direct observation of OM mechanics, which has been done only on large saccular otolith of fish (de Vries 1950). Preliminary direct observations in mammals suggests that the estimate of τ_1 from afferent discharge is much too large (J.W. Grant, personal communication); should this be confirmed, otolith organs would remain acceleration sensors to very high frequencies. In the derivation, we have assumed that stiffness resides in the OM and have ignored the possibly major contribution of hair bundles (Benser et al. 1993).

We have also assumed that the GL and CL had identical properties. Given the differences in their structure, it would seem reasonable to assume that virtually all of the shear deformation takes place in the CL. The main effect is to increase the calculated values of E and μ and to reduce the overall displacement of the OM. Another simplifying assumption is that each macula lies in a single plane. This is clearly not the case as both organs show curvature. How this affects directional properties will depend on the mechanical properties of the GL. Were the GL perfectly rigid, the OM should move as a unit and polarization vectors should all lie in a single plane. If, on the other hand, the GL were perfectly compliant, each point in the OM should behave independently with its polarization vector being parallel to the local plane. The issue has been explored with finite-element models (Jaeger et al. 2002; Kondrachuk 2001a), which suggest that vectors are predominantly influenced by local orientation. Obviously, these issues bear on the complementary roles played by the utricular and saccular maculae. In a previous section, we suggested that the utricular macula encoded information about linear forces acting in the horizontal plane, whereas the saccular macula handled vertically oriented forces. If, in fact, directional properties are mainly influenced by local orientation, units innervating the anterior, upwardly curving portion of the utricular macula should be sensitive to vertical forces. Given the curvature of the saccular macula

(Lindeman 1969), some of its units might be sensitive to horizontally oriented forces. In short, while the major planes of the two maculae have complementary directional properties, both organs could potentially have overlapping directional properties.

Afferent Response Dynamics

Because the utricular and saccular maculae have similar structures, we might expect the two organs to have similar response dynamics. This has been confirmed in afferent recordings (Fernández and Goldberg 1976c). For either organ, there are differences between regular and irregular otolith afferents. As was the case for the cristae, regular otolith afferents have response dynamics resembling those expected of macromechanics, while irregular units show large discrepancies from expectations.

Bode plots for the two kinds of otolith afferents are shown in Figure 4.23. For regular units, the gain re linear acceleration is almost constant from dc to 2 Hz. Responses are nearly in phase with linear acceleration, small phase leads being replaced by larger phase lags as frequency is increased. The low-frequency phase lead may be due to adaptive processes, at least partly located in the afferent terminal, while the high-frequency phase lag is interpreted, with some reservations, as reflecting macromechanics. In contrast to the relatively flat response dynamics of regular units, there is an approximately 10-fold frequency-dependent increase in gain for irregular units and conspicuous phase leads at all frequencies. These latter effects can be explained by the irregular units, besides sharing the adaptive and mechanical processes of regular units, being sensitive to the velocity of otolith displacement, as well as to the displacement itself. Were the response simply proportional to otolith velocity, we would expect that at some point the gain would increase linearly with stimulus frequency (f) and the phase would approach 90 degrees. Neither is the case. Rather, gain increases as the one-third power of frequency ($f^{1/3}$) and phase

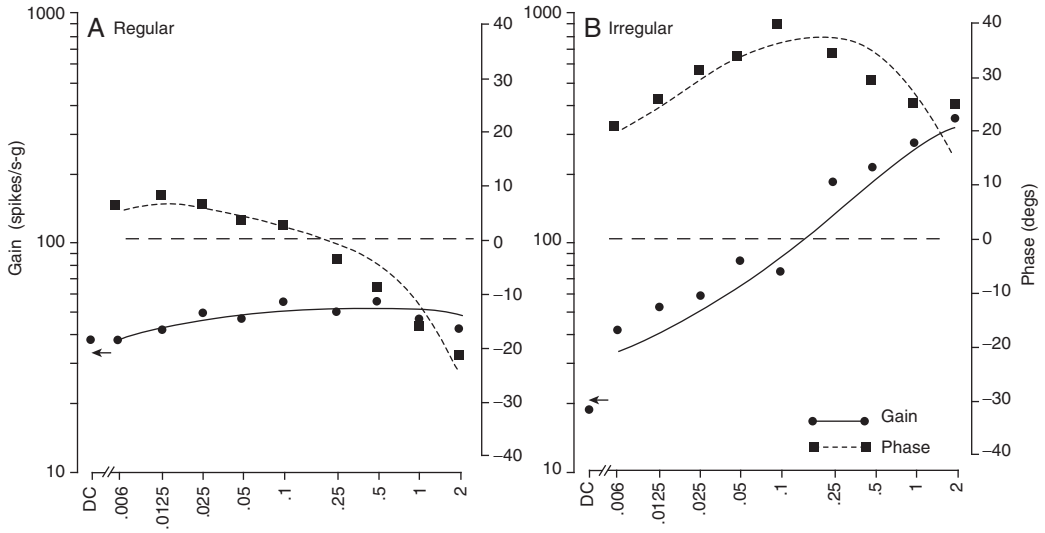

Figure 4.23 Response dynamics for two otolith afferents in the squirrel monkey. Gains (left ordinate, *solid line*) and phases (right ordinate, *dashed line*) re linear force versus sinusoidal frequency for a regular unit (**A**) and an irregular unit (**B**). The irregular unit has more phasic response dynamics as indicated by its larger phase leads and its larger high-frequency gain enhancement. Curves are from empirical transfer functions, with *arrows* indicating predicted static (DC) gains. Dashed horizontal lines indicate zero phase. (From Fernández and Goldberg 1976c)

straddles 30 degrees. These are hallmarks of a fractional-differential operator (Oldham and Spannier 2006; Thorson and Biederman-Thorson 1974).

Response dynamics can also be illustrated by the responses to linear-force trapezoids. Trapezoids are presented that differ in the durations of their ascending and descending ramps, but not in their plateau duration or magnitude. For a regular unit (Fig. 4.24A,B), the peak responses are almost identical regardless of the velocity of force application, illustrating that the unit is almost exclusively sensitive to the instantaneous force. In contrast, an irregular unit shows velocity sensitivity: peak response is considerably larger during the faster (Fig. 4.24C) than during the slower force application (Fig. 4.24D). Were response proportional to velocity, we would expect an instantaneous step increase in discharge during the ramp and an instantaneous step fall on ramp termination. Both the increase in discharge during the ramp and its decline during the plateau are more gradual than this, features that are consistent with a fractional operator.

Dynamic Range of Afferent Discharge

To determine the dynamic ranges of otolith afferents, responses to centrifugal forces over a

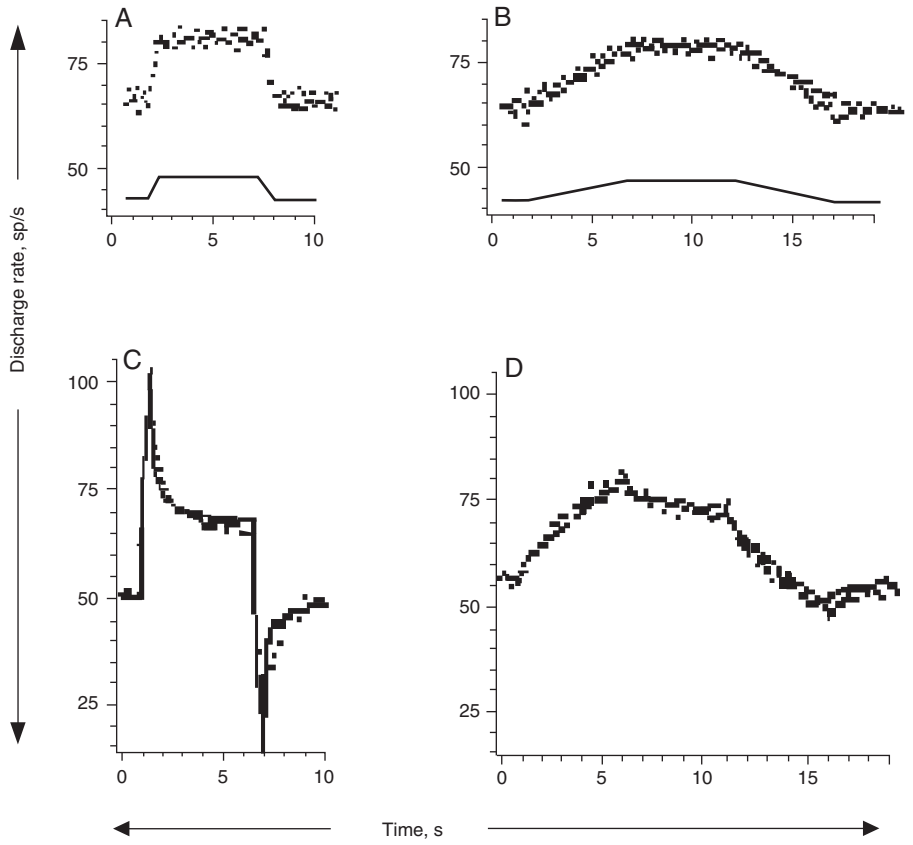

Figure 4.24 Responses to linear force for a regular unit (**A, B**) and an irregular unit (**C, D**). Two force trapezoids whose ramps differ in their durations and slopes are presented to each unit. The regular unit responds to force magnitude, but not to the rate of force application. Two components are seen in the irregular unit, one proportional to the rate of force application, the other to force magnitude. Curves are predicted responses based on transfer functiond with fractionsl operators. (From Fernández and Goldberg 1976c)

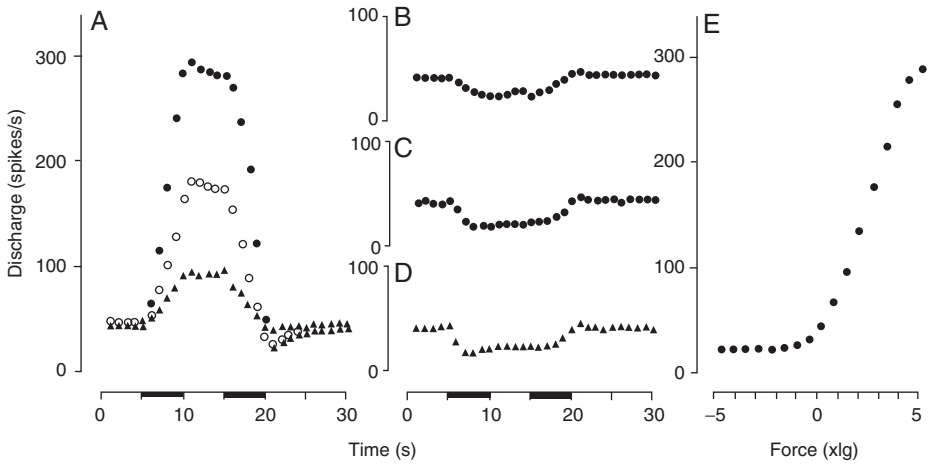

Figure 4.25 Responses of a regular otolith afferent to force trapezoids. **A**. Excitatory response profiles: 1.23 g (⑩); 2.46 g (④); and 4.92 g (③) force plateaus. **B–D**. Inhibitory response profiles for 1.23, 2.46, and 4.92 g force plateaus, respectively. **E**. Force–response relation. Note that the unit continues to fire during inhibitory saturation. (From Fernández and Goldberg 1976b)

range of ±4.92 g were studied (Fernández and Goldberg 1976b). This was done only in regular afferents. An example is seen in Figure 4.25. Responses are asymmetric. As excitatory force is increased, responses continue to grow with discharge approaching 300 spikes/s (Fig. 4.25A). In contrast, even modest inhibitory responses saturate so that increasing force does not reduce discharge below a residual discharge of 17 spikes/s (Fig. 4.25B–D). The overall input–output relation is sigmoidal (Fig. 4.25E). Maximum sensitivity occurs at an inflection points displaced 2.4 g in the excitatory direction from zero force. The range of ±1 g is located in the lower, concave upward part of the relation and is characterized by a sensitivity of 28 spikes•s^{-1}/g, some 40% of the maximum sensitivity.

Data for this and other units are well fit by first-order Boltzmann functions (Fig. 4.26)

$$r(x) = \frac{1}{1 + \exp[-(x - x_0)/s]} \qquad (4.13)$$

where $r(x)$ is the response to a force (x), x_0 is the force at the inflection point, and s is a sensitivity factor. The dynamic range can be defined by the two points along the stimulus axis leading to 10% and 90% of the maximum response. For the particular unit of Fig. 4.25, the points are 0.34 g (10%) and 4.4 g (90%), leading to a dynamic range of 4.0 g. Average values (±SD) based on all the units in Figure 4.26 are –0.58 ± 0.77 g (10%), 4.0 ± 0.96 g (90%), and 4.6 ± 1.1 g (dynamic range). The dynamic range in the

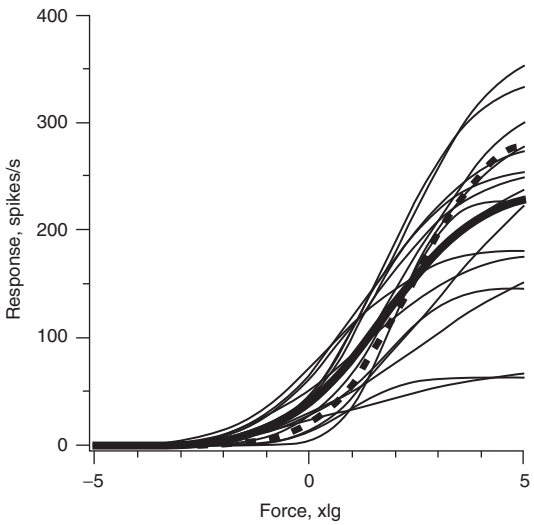

Figure 4.26 Relations between response and force. Each thin curve is the best-fitting Boltzmann relation (Equation 4.13) for an individual, regularly discharging unit. Responses are measured from the minimum rate obtained during large inhibitory forces. Thick lines indicate relation for unit illustrated in Figure 4.24 (- - -) and relation based on average parameters for all units (—). (Based on Fernández and Goldberg 1976b)

larger population extends well beyond ±1 g, the range needed to encode static tilts. At the same time, there is considerable variation in the maximal discharge of individual units.

Variations in Gain and Phase

As already noted, regular and irregular units differ in their response dynamics (see Figs. 4.23 and 4.24). This is reflected by the fact that both the 2-Hz gain (g_{2Hz}) and phase (φ_{2Hz}), obtained from extracellularly recorded units (Fig. 4.27A,B), increase with cv*. Although similar trends are seen in canal units (see Fig. 4.15), there are obvious differences between the two data sets. As was true for canal units, there is a single, semilogarithmic relation between phase and cv* (Fig. 4.27B). But unlike the case for canal units, g_{2Hz} for irregular utricular units does not fall into two discrete clusters (Fig. 4.27A). Another difference may be noted. In both kinds of organs, the response dynamics of regular and irregular afferents deviate from each other. The deviations fall into distinct low- and high-frequency ranges for canal units (see Fig. 4.12 and 4.13) but are broadly distributed across the frequency range for otolith units (see Fig. 4.23).

Afferent Morphology and Physiology

Intra-axonal labeling studies have been done for utricular afferents in the chinchilla (Goldberg et al. 1990b). For the labeled afferents, polarization vectors were determined by static tilts. The locations and vectors of the labeled units were compared with published morphological-polarization maps (see Fig. 2.9). The great majority of labeled units had vectors consistent with the maps. As expected from extracellular labeling studies (see Fig. 2.14), intra-axonally labeled calyx units were found exclusively in the striola, while dimorphic units were found in the striola, juxtastriola, and extrastriola. None of the labeled units were of the bouton variety. Their absence from the sample is hardly surprising considering that they have small axons and make up only ≈10% of the total innervation.

Calyx units are the most irregularly discharging units in the sample (Fig. 4.27C,D). The discharge regularity of dimorphic units depends on their location. Most of those located in the striola are irregular, whereas most peripheral extrastriolar dimorphs are regular. Juxtastriolar dimorphs, lying adjacent to the striola, are neither as regular as the most regularly discharging units in the peripheral extrastriola nor as irregularly discharging as some striolar dimorphic or calyx units. The relation between linear-force gain ($g_{2\ Hz}$) and discharge regularity (cv*) and that between the phase of the linear-force response (Φ_{2Hz}) and cv* were similar for the extracellular (Fig. 4.27A,B) and intra-axonal samples (Fig. 4.27C,D). There is a single, semilogarithmic relation between phase and cv* for the intra-axonal sample, including dimorphic and calyx units. In addition, a strong, nearly linear relation exists in the intra-axonal sample between $g_{2\ Hz}$ and cv* for regular dimorphic units (cv* ≤ 0.1). Many irregular units have relatively high gains, but none of the gains are as high as would be suggested from an extrapolation of the power-law for regular units. In addition, there is no clear separation in the values of g_{2Hz} for calyx and irregular dimorphic units. This is in contrast to data from the semicircular canals in which calyx units have distinctively low 2-Hz gains. The low gains of calyx units in the canals suggested that synaptic inputs from type I hair cells were smaller than expected from the number of synaptic contacts with calyx inner faces. In an attempt to retain the hypothesis for the macula, it has been suggested that the comparable 2-Hz gains of utricular calyx and irregular dimorphs can be explained by the former units having a somewhat more irregular discharge and more phasic response dynamics (for details, see Goldberg et al. 1990b).

We can summarize the results as follows. Calyx afferents, which are confined to the striola, are the most irregularly discharging afferents, and their responses to 2-Hz sinusoidal linear forces are characterized by high gains and the largest phase leads. Dimorphic afferents, which are found throughout the macula, provide evidence for a regional variation in discharge properties. Striolar dimorphs are distinguished from extrastriolar dimorphs in having a more irregular discharge, higher gains, and larger phases. In all these respects, juxtastriolar dimorphs show intermediate properties. As already noted, no physiologically characterized bouton fibers were recovered. Based on their

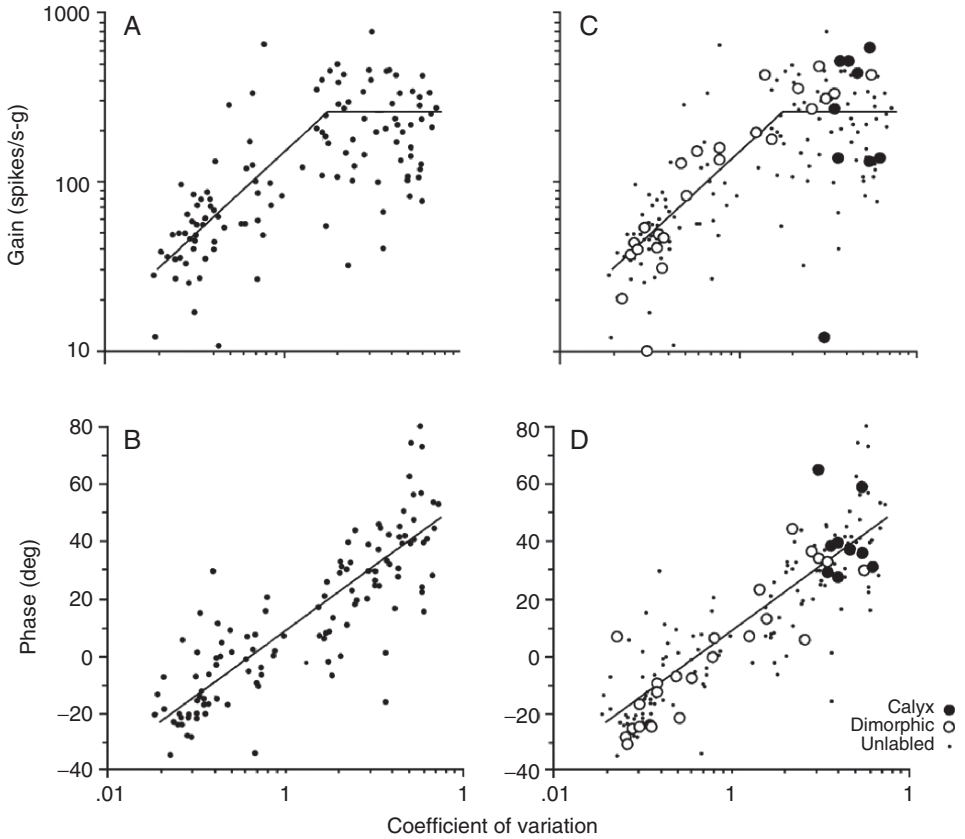

Figure 4.27 Gains and phases versus normalized coefficient of variation (cv*). Utricular afferents in the chinchilla responding to 2-Hz sinusoidal centrifugal forces parallel to each unit's polarization vector. Each point represents one unit. **A, B.** Extracellularly recorded units. *Sloping line* in **A** is best-fitting power law relation between gain and cv* for units, cv* < 0.18. *Horizontal line* indicates average gain for units, cv* > 0.18. *Straight line* in **B** is best-fitting semilogarithmic relation between phase and cv* for all units. **C, D**. Corresponding data for intracellularly labeled units, including 24 dimorphic and 9 calyx units (see Key). Unlabeled units are shown as *small dots*. Calyx units are the most irregularly discharging afferents and have the largest phase leads; their gains are not distinctive. Gains and phases of dimorphic units increase in association with cv*; regular units are found in the extrastriola and irregular units in the striola. (From Goldberg et al. 1990b)

location in the peripheral extrastriola, they might be expected to have a regular discharge, low gains, and small phases. In the canals, calyx afferents have distinctively low gains compared to irregular dimorphs also located in the central zone. This is not the case for utricular macula, but the results do not disprove the proposition that calyx endings are associated with a lower synaptic gain than would be predicted from the number of synapses they make with hair cells.

We now consider a functional correlate of the difference between the canal and otolith calyx afferents. In the case of the canals, it has been suggested that the gains of calyx afferents would allow these irregular units to respond linearly to even very rapid head saccades. In contrast, the linear accelerations occurring during everyday

activity are of limited magnitude, less than 1 g for walking and less than 2 g for running and hopping (Pozzo et al. 1990). Similar stimulus magnitudes occur during non-locomotor activities (MacDougall and Moore 2005). Maximal gains of irregular otolith afferents, whether calyx or dimorphic, are near 300 spikes•s^{-1}/g^{-1} for high-frequency linear forces (Angelaki and Dickman 2000; Fernández and Goldberg 1976c; Goldberg et al. 1990a) (see Fig. 4.23). Peak excitatory responses should be on the order of 400 spikes/s, within the upper response limits of many otolith afferents.

4.4 SUMMARY

Semicircular canals provide a three-dimensional reconstruction of angular forces acting on the head, while otolith afferents do the same for linear forces. Afferents have a resting discharge, whose presence allows bidirectional responses, effectively eliminates the existence of a sensory threshold, and provides a tonic excitatory input to central vestibular pathways. Fibers, whether they innervate canal or otolith organs, differ in discharge regularity, which is largely determined by the physiology of the spike encoder located in the postsynaptic terminal. Irregular afferents are more sensitive than are regular afferents to afferent and efferent synaptic inputs and to externally applied galvanic stimulation. Response dynamics of regular afferents resemble the expected biomechanics of cupular or otolithic displacement, whereas irregular afferents show more phasic response dynamics. Differences in response dynamics, while correlated with discharge regularity, cannot be explained by variations in encoder sensitivity.

Each semicircular canal responds to head rotations having a component near the canal plane. The discharge of all afferents innervating a crista is increased by rotations in one and the same direction and decreased by rotations in the other direction. Coplanar canal pairs on the two sides have opposite directional properties. It is the difference in activity of coplanar canal pairs that is interpreted by the brain as a rotation. The biomechanics of the semicircular canals follows that of an overdamped torsion pendulum whose response dynamics incorporates the effects of endolymph inertia and viscosity and of cupular elasticity. Throughout a broad frequency range (0.025 to 25 Hz), viscosity dominates and cupular displacement is proportional to angular head velocity. The response properties of dimorphic units vary with location. Those in the peripheral zone are regularly discharging and have low rotational gains and tonic response dynamics. Bouton units are located in the peripheral zone of the crista and may be presumed to resemble their dimorphic neighbors. Calyx units, which innervate the central zone of the crista, are the most irregular and most phasic afferents and have lower gains for mid-frequency rotations than do similarly located irregular dimorphs.

The directional properties of each otolith afferent can be summarized by a functional polarization vector. Since otolith organs respond to shearing but not to compressional forces, most utricular afferents respond to linear forces in the horizontal plane, whereas most saccular afferents are sensitive to dorsoventral forces. The biomechanics of the otoconial membrane acts like a first-order system that is sensitive to linear acceleration below a corner frequency that still needs to be determined and to linear velocities above it. Striolar otolith afferents are irregularly discharging and phasic and have high gains to linear accelerations, whereas peripheral extrastriolar units are regularly discharging and tonic and have low gains. Striolar calyx units are more irregular and more phasic than similarly located dimorphic afferents. Unlike calyx units in the semicircular canals, those in the utricular macula do not have distinctively low gains. From a functional perspective, the difference in calyx gains may be related to the range of stimulus magnitudes handled by canal and otolith organs.

4.5 SELECTED READINGS

Eatock RA, Lysakowski A (2006) Mammalian vestibular hair cells. In: Vertebrate Hair Cells (Eatock RA, Fay RR, Popper AN, eds), pp. 348–442. Berlin: Springer-Verlag.

Goldberg JM (2000) Afferent diversity and the organization of central vestibular pathways. Exp Brain Res 130:277–297.

Highstein SM, Rabbitt RD, Holstein GR, Boyle RD (2005) Determinants of spatial and temporal coding by semicircular canal afferents. J Neurophysiol 93:2359–2370.

Lewis ER, Leverenz EL, Bialek WS (1985) The Vertebrate Inner Ear. Boca Raton FL: CRC Press.
Lysakowski A, Goldberg JM (2004) Morphophysiology of the vestibular periphery. In: The Vestibular System (Highstein SM, Popper A, Fay RR, eds), pp. 57–152. New York: Springer-Verlag.
Rabbitt RD, Damiano ER, Grant JW (2004a) Biomechanics of the semicircular canals and otolith organs. In: The Vestibular System (Highstein SM, Popper A, Fay RR, eds), pp. 153–201. New York: Springer-Verlag.

REFERENCES

Alberts BM, Roberts K, Lewis J, Raff M, Walter P, Johnson A (2002) Molecular Biology of the Cell, 4th ed. New York: Garland Science.
Anastasio TJ, Correia MJ, Perachio AA (1985) Spontaneous and driven responses of semicircular canal primary afferents in the unanesthetized pigeon. J Neurophysiol 54:335–347.
Anderson JH, Blanks RHI, Precht W (1978) Response characteristics of semicircular canal and otolith systems in the cat. I. Dynamic responses of primary vestibular fibers. Exp Brain Res 32: 491–507.
Angelaki DE (1992) Two-dimensional coding of linear acceleration and the angular velocity sensitivity of the otolith system. Biol Cybern 67:511–521.
Angelaki DE, Bush GA, Perachio AA (1993) Two-dimensional spatiotemporal coding of linear acceleration in vestibular nuclei neurons. J Neurosci 13:1403–1417.
Angelaki DE, Dickman JD (2000) Spatiotemporal processing of linear acceleration: primary afferent and central vestibular neuron responses. J Neurophysiol 84:2113–2132.
Angelaki DE, Shaikh AG, Green AM, Dickman JD (2004) Neurons compute internal models of the physical laws of motion. Nature 430:560-564.
Armand M, Minor LB (2001) Relationship between time- and frequency-domain analyses of angular head movements in the squirrel monkey. J Comput Neurosci 11:217–239.
Baird RA (1994) Comparative transduction mechanisms of hair cells in the bullfrog utriculus. II. Sensitivity and response dynamics to hair bundle displacement. J Neurophysiol 71:685–705.
Baird RA, Desmadryl G, Fernández C, Goldberg JM (1988) The vestibular nerve of the chinchilla. II. Relation between afferent response properties and peripheral innervation patterns in the semicircular canals. J Neurophysiol 60:182–203.
Bárány R (1906) Untersuchungen über den vom-Vestibularapparat des Ohres reflektorisch ausgelosten rythmischen Nystagmus und seine Begleiterscheinungen. Mschr Ohrenheilkd 40: 193–297.
Benser ME, Issa NP, Hudspeth AJ (1993) Hair-bundle stiffness dominates the elastic reactance to otolithic-membrane shear. Hear Res 68:243–252.
Blanks RH, Curthoys IS, Bennett ML, Markham CH (1985) Planar relationships of the semicircular canals in rhesus and squirrel monkeys. Brain Res 340:315–324.
Blanks RH, Curthoys IS, Markham CH (1972) Planar relationships of semicircular canals in the cat. Am J Physiol 223:55–62.
Blanks RH, Precht W (1978) Response properties of vestibular afferents in unanesthetized cats during optokinetic and vestibular stimulation. Neurosci Lett 10:225–229.
Borst A, Theunissen FE (1999) Information theory and neural coding. Nat Neurosci 2:947–957.
Boyle R, Carey JP, Highstein SM (1991) Morphological correlates of response dynamics and efferent stimulation in horizontal semicircular canal afferents of the toadfish, *Opsanus tau*. J Neurophysiol 66:1504–1521.
Boyle R, Highstein SM (1990) Resting discharge and response dynamics of horizontal semicircular canal afferents in the toadfish, *Opsanus tau*. J Neurosci 10:1557–1569.
Bronte-Stewart HM, Lisberger SG (1994) Physiological properties of vestibular primary afferents that mediate motor learning and normal performance of the vestibulo-ocular reflex in monkeys. J Neurosci 14: 1290-1308.
Breuer J (1874) Ueber die Function der Bogengänge des Ohrlabyrinths. Wien Med Jahrb:72–124.
Breuer J (1875) Beiträge zur Lehre von statischen Sinne. Wien Med Jahrb:87–156.
Brichta AM, Goldberg JM (2000a) Morphological identification of physiologically characterized afferents innervating the turtle posterior crista. J Neurophysiol 83:1202–1223.
Bush GA, Perachio AA, Angelaki DE (1993) Encoding of head acceleration in vestibular neurons. I. Spatiotemporal response properties to linear acceleration. J Neurophysiol 69:2039–2055.
Calabrese DR, Hullar TE (2006) Planar relationships of the semicircular canals in two strains of mice. J Assoc Res Otolaryngol 7:151-159.
Carlström D (1963) A crystallographic study of vertebrate otoliths. Biol Bull 125:441–463.
Clark B (1967) Thresholds for the perception of angular acceleration in man. Aerospace Med 38:443–450.
Coats AC, Smith SY (1967) Body position and the intensity of caloric nystagmus. Acta Otolaryngol (Stockh) 63:515–532.
Correia MJ, Perachio AA, Dickman JD, Kozlovskaya IB, Sirota MG, Yakushin SB, Beloozerova IN (1992) Changes in monkey horizontal semicircular canal afferent responses after spaceflight. J Appl Physiol 73:112S-120S.
Crum Brown A (1874) On the semicircular canals of the internal ear. J Anat Physiol.

Curthoys IS (1982) The response of primary horizontal semicircular canal neurons in the rat and guinea pig to angular acceleration. Exp Brain Res 47:286–294.

Curthoys IS, Curthoys EJ, Blanks RH, Markham CH (1975) The orientation of the semicircular canals in the guinea pig. Acta Otolaryngol 80:197–205.

Curthoys IS, Oman CM (1986) Dimensions of the horizontal semicircular duct, ampulla and utricle in rat and guinea pig. Acta Otolaryngol (Stockh) 101:1–10.

de Vries H (1950) The mechanics of the labyrinthine otoliths. Acta Otolaryngol (Stockh) 38:262–273.

Dingledine R, Borges K, Bowie D, Traynelis SF (1999) The glutamate receptor ion channels. Pharmacol Rev 51:8–61.

Dohlman GF (1935) Some practical and theoretical points in labyrinthology. Proc Roy Soc Med: 1371–1380.

Dohlman GF (1971) The attachment of the cupulae, otolith and tectorial membranes to the sensory cell areas. Acta Otolaryngol (Stockh) 71:89–105.

Dunlap M, Spoon C, Grant JW (2011) Dynamic response of the otoconial membrane of the turtle utricle. Assoc. Res. Otolaryngol. Abs. (in press).

Eatock RA, Lysakowski A (2006) Mammalian vestibular hair cells. In: Vertebrate Hair Cells (Eatock RA, Fay RR, Popper AN, eds), pp. 348–442. Berlin: Springer-Verlag.

Edwards CH, Penney DE (2000) Elementary Differential Equations with Boundary Value Problems. Upper Saddle River, NJ: Prentice Hall.

Estes MS, Blanks RH, Markham CH (1975) Physiologic characteristics of vestibular first-order canal neurons in the cat. I. Response plane determination and resting discharge characteristics. J Neurophysiol 38:1232–1249.

Ezure K, Cohen MS, Wilson VJ (1983) Response of cat semicircular canal afferents to sinusoidal polarizing currents: implications for input-output properties of second-order neurons. J Neurophysiol 49:639–648.

Fernández C, Goldberg JM (1971) Physiology of peripheral neurons innervating semicircular canals of the squirrel monkey. II. Response to sinusoidal stimulation and dynamics of peripheral vestibular system. J Neurophysiol 34:661–675.

Fernández C, Goldberg JM (1976a) Physiology of peripheral neurons innervating otolith organs of the squirrel monkey. I. Response to static tilts and to long-duration centrifugal force. J Neurophysiol 39:970–984.

Fernández C, Goldberg JM (1976b) Physiology of peripheral neurons innervating otolith organs of the squirrel monkey. II. Directional selectivity and force-response relations. J Neurophysiol 39:985–995.

Fernández C, Goldberg JM (1976c) Physiology of peripheral neurons innervating otolith organs of the squirrel monkey. III. Response dynamics. J Neurophysiol 39:996–1008.

Fernández C, Goldberg JM, Abend WK (1972) Response to static tilts of peripheral neurons innervating otolith organs of the squirrel monkey. J Neurophysiol 35:978–987.

Furukawa T, et al. (1982) Quantal analysis of a decremental response at hair cell -afferent fibre synapse in the goldfish sacculus. J Physiol (Lond) 322: 181–195.

Furukawa T, Matsuura S (1978) Adaptive rundown of excitatory post-synaptic potentials at synapses between hair cells and eight nerve fibres in the goldfish. J Physiol (Lond) 276:193–209.

Goldberg JM (2000) Afferent diversity and the organization of central vestibular pathways. Exp Brain Res 130:277–297.

Goldberg JM, Brichta AM (2002b) Functional analysis of whole cell currents from hair cells of the turtle posterior crista. J Neurophysiol 88:3279–3292.

Goldberg JM, Desmadryl G, Baird RA, Fernández C (1990a) The vestibular nerve of the chinchilla. IV. Discharge properties of utricular afferents. J Neurophysiol 63:781–790.

Goldberg JM, Desmadryl G, Baird RA, Fernandez C (1990b) The vestibular nerve of the chinchilla. V. Relation between afferent discharge properties and peripheral innervation patterns in the utricular macula. J Neurophysiol 63:791–804.

Goldberg JM, Fernandez C (1971a) Physiology of peripheral neurons innervating semicircular canals of the squirrel monkey. I. Resting discharge and response to constant angular accelerations. J Neurophysiol 34:635–660.

Goldberg JM, Fernandez C (1971b) Physiology of peripheral neurons innervating semicircular canals of the squirrel monkey. III. Variations among units in their discharge properties. J Neurophysiol 34:676–684.

Goldberg JM, Fernandez C (1975) Responses of peripheral vestibular neurons to angular and linear accelerations in the squirrel monkey. Acta Otolaryngol (Stockh) 80:101–110.

Goldberg JM, Fernandez C (1977) Conduction times and background discharge of vestibular afferents. Brain Res 122:545–550.

Goldberg JM, Fernandez C, Smith CE (1982) Responses of vestibular-nerve afferents in the squirrel monkey to externally applied galvanic currents. Brain Res 252:156–160.

Goldberg JM, Smith CE, Fernández C (1984) Relation between discharge regularity and responses to externally applied galvanic currents in vestibular nerve afferents of the squirrel monkey. J Neurophysiol 51:1236–1256.

Goltz F (1870) Ueber die physiologische Bedeutung der Bogengange der Ohrlabytinths. Pflugers Archiv Eur J Physiol 3:172–192.

Goodyear RJ, Richardson GP (2002) Extracellular matrices associated with the apical surfaces of sensory epithelia in the inner ear: molecular and structural diversity. J Neurobiol 53:212–227.

Au:- Please let me know if there is any update?

Goutman JD, Glowatzki E (2007) Time course and calcium dependence of transmitter release at a single ribbon synapse. Proc Natl Acad Sci U S A 104:16341–16346.

Grant JW, Best WA (1986) Mechanics of the otolith organ—dynamic response. Ann Biomed Eng 14:241–256.

Grant JW, Cotton JR (1990) A model for otolith dynamic response with a viscoelastic gel layer. J Vestib Res 1:139–151.

Grant JW, Huang CC, Cotton JR (1994) Theoretical mechanical frequency response of the otolithic organs. J Vestib Res 4:137–151.

Grossman GE, Leigh RJ, Abel LA, Lanska DJ, Thurston SE (1988) Frequency and velocity of rotational head perturbations during locomotion. Exp Brain Res 70:470–476.

Guedry FE, Jr. (1974) Psychophysics of vestibular sensation. In: Handbook of Sensory Physiology. Volume VI. Vestibular System. Part 2: Psychophysics, Applied Aspects and General Interpretations (Kornhuber HH, ed), pp. 3–154. Berlin: Springer-Verlag.

Guth PS, Perrin P, Norris CH, Valli P (1998) The vestibular hair cells: post-transductional signal processing. Prog Neurobiol 54:193–247.

Haque A, Angelaki DE, Dickman JD (2004) Spatial tuning and dynamics of vestibular semicircular canal afferents in rhesus monkeys. Exp Brain Res 155:81–90.

Highstein SM, Rabbitt RD, Boyle R (1996) Determinants of semicircular canal afferent response dynamics in the toadfish, *Opsanus tau*. J Neurophysiol 75:575–596.

Highstein SM, Rabbitt RD, Holstein GR, Boyle RD (2005) Determinants of spatial and temporal coding by semicircular canal afferents. J Neurophysiol 93:2359–2370.

Hillman DE, McLaren JW (1979) Displacement configuration of semicircular canal cupulae. Neuroscience 4:1989–2000.

Hirsch-Shell D. Paulin M, Hoffman L (2011) The contributions of signal and noise to information transmission rates in mammalian vestibular afferent neurons. Assoc Res Otolaryngol Abs: 761.

Holstein GR, Martinelli GP, Henderson SC, Friedrich VL, Jr., Rabbitt RD, Highstein SM (2004a) Gamma-aminobutyric acid is present in a spatially discrete subpopulation of hair cells in the crista ampullaris of the toadfish *Opsanus tau*. J Comp Neurol 47:1–10.

Holstein GR, Rabbitt RD, Martinelli GP, Friedrich VLJ, Boyle R, Highstein SM (2004b) Covergence of excitatory and inhibitory hair cell transmitter shapes vestibular afferent responses. Proc Natl Acad Sci U S A 101.

Holt JR, Corey DP, Eatock RA (1997) Mechanoelectric transduction and adaptation in hair cells of the mouse utricle, a low-frequency vestibular organ. J Neurosci 17:8739–8748.

Holt JC, Xue J-T, Brichta AM, Goldberg JM (2006b) Transmission between type II hair cells and bouton afferents in the turtle posterior crista. J Neurophysiol 95:428–452.

Honrubia V, Hoffman LF, Sitko S, Schwartz IR (1989) Anatomic and physiological correlates in bullfrog vestibular nerve. J Neurophysiol 61:688–701.

Hullar TE, Della Santina CC, Hirvonen T, Lasker DM, Carey JP, Minor LB (2005) Responses of irregularly discharging chinchilla semicircular canal vestibular-nerve afferents during high-frequency head rotations. J Neurophysiol 93: 2777–2786.

Hullar TE, Minor LB (1999) High-frequency dynamics of regularly discharging canal afferents provide a linear signal for angular vestibuloocular reflexes. J Neurophysiol 82:2000–2005.

Hunter-Duvar IM, Hinajosa R (1984) Vestibule: sensory epithelia. In: Ultrastructural Atlas of the Inner Ear (Friedmann I, Ballantyne J, eds), pp. 211–244. London: Butterworths.

Huterer M, Cullen KE (2002) Vestibuloocular reflex dynamics during high-frequency and high-acceleration rotations of the head on body in rhesus monkey. J Neurophysiol 88:13–28.

Igarashi M (1967) Dimensional study of the vestibular apparatus. Laryngoscope 77:1806–1817.

Jaeger R, Takagi A, Haslwanter T (2002) Modeling the relation between head orientations and otolith responses in humans. Hear Res 173:29–42.

Jones GM, Spells KE (1963) A theoretical and comparative study of the functional dependence of the semicircular canal upon its physical dimensions. Proc Roy Soc London B 157:403–419.

Kachar B, Parakkal M, Fex J (1990) Structural basis for mechanical transduction in the frog vestibular sensory apparatus: I. The otolithic membrane. Hear Res 45:179–190.

Kachar B, Parakkal M, Kurc M, Zhao Y, Gillespie PG (2000) High-resolution structure of hair-cell tip links. Proc Natl Acad Sci U S A 97:13336–13341.

Keller EL (1976) Behavior of horizontal semicircular canal afferents in alert monkey during vestibular and optokinetic stimulation. Exp Brain Res 24:459–471.

Kondrachuk AV (2001a) Finite element modeling of the 3D otolith structure. J Vestib Res 11:13–32.

Kondrachuk AV (2001b) Models of the dynamics of otolithic membrane and hair cell bundle mechanics. J Vestib Res 11:33–42.

Kondrachuk AV (2002) Otoliths as biomechanical gravisensors. Adv Space Res 30:745–750.

Lewis ER, Leverenz EL, Bialek WS (1985) The Vertebrate Inner Ear. Boca Raton FL: CRC Press.

Liao K, Kumar AN, Han YH, Grammer VA, Gedeon BT, Leigh RJ (2005) Comparison of velocity waveforms of eye and head saccades. Ann N Y Acad Sci 1039:477–479.

Lim DJ (1976) Morphological and physiological correlates in cochlear and vestibular sensory epithelia.

In: Scanning Electron Microscopy/1976/II. Chicago: Illinois Institute of Technology Research Institute.

Lim DJ (1984) The development and structure of the otoconia. In: Ultrastructural Atlas of the Inner Ear (Friedmann I, Ballantyne J, eds), pp. 245–269. London: Butterworths.

Lindeman HH (1969) Studies on the morphology of the sensory regions of the vestibular apparatus. Ergebnisse Anatomie Entwicklungsgeschite 42:1–113.

Lisberger SG, Pavelko TA (1986) Vestibular signals carried by pathways subserving plasticity of the vestibulo-ocular reflex in monkeys. J Neurosci 6:346–354.

Loe PR, Tomko DL, Werner G (1973) The neural signal of angular head position in primary afferent vestibular nerve axons. J Physiol (Lond) 230: 29–50.

Louie AW, Kimm J (1976) The response of 8th nerve fibers to horizontal sinusoidal oscillation in the alert monkey. Exp Brain Res 24:447–457.

Lowenstein O, Sand A (1936) The activity of the horizontal semicircular canal of the dogfish, *Scyllium canalicula*. J Exp Biol 13:416–428.

Lowenstein O, Sand A (1940a) The individual and integrated activity of the semicircular canals of the elasmobranch labyrinth. J Physiol (Lond) 99: 89–101.

Lowenstein O, Wersäll J (1954) A functional interpretation of the electron microscopic structure of the sensory hairs in the cristae of the elasmobranch, *Raja clavata*. Nature 184:1807–1810.

Lundberg YW, Zhao X, Yamoah EN (2006) Assembly of the otoconia complex to the macular sensory epithelium of the vestibule. Brain Res 1091: 47–57.

Lysakowski A (1996) Synaptic organization of the crista ampullaris in vertebrates. Ann N Y Acad Sci 781:164–182.

Lysakowski A, Goldberg JM (1997) A regional ultrastructural analysis of the cellular and synaptic architecture in the chinchilla cristae ampullares. J Comp Neurol 389:419–443.

Lysakowski A, Goldberg JM (2004) Morphophysiology of the vestibular periphery. In: The vestibular system (Highstein SM, Popper A, Fay RR, eds), pp. 57–152. New York: Springer-Verlag.

Lysakowski A, Goldberg JM (2008) Ultrastructural analysis of the cristae ampullares in the squirrel monkey (*Saimiri sciureus*). J Comp Neurol 511: 47–64.

Lysakowski A, Minor LB, Fernández C, Goldberg JM (1995) Physiological identification of morphologically distinct afferent classes innervating the cristae ampullares of the squirrel monkey. J Neurophysiol 73:1270–1281.

MacDougall HG, Moore ST (2005) Marching to the beat of the same drummer: the spontaneous tempo of human locomotion. J Appl Physiol 99:1164–1173.

Mach E (1874) Physicalische Versuche über den Gleichgewichtssinn des Menschen. Wien Sitzb Kais Akad Wiss 69:121–135.

Matano S (1986) A volumetric comparison of the vestibular nuclei in primates. Folia Primatol (Basel) 47:189–203.

Melvill Jones G (1974) The functional significance of semicircular canal size. In: Handbook of Sensory Physiology. Volume VI. Vestibular System. Part 1: Basic Mechanisms (Kornhuber HH, ed), pp. 171–184. Berlin: Springer-Verlag.

Minor LB, Goldberg JM (1990) Influence of static head position on the horizontal nystagmus evoked by caloric, rotational and optokinetic stimulation in the squirrel monkey. Exp Brain Res 82:1–13.

Minor LB, Lasker DM, Backous DD, Hullar TE (1999) Horizontal vestibuloocular reflex evoked by high-acceleration rotations in the squirrel monkey. I. Normal responses. J Neurophysiol 82:1254–1270.

Myers SF, Lewis ER (1990) Hair cell tufts and afferent innervation of the bullfrog crista ampullaris. Brain Res 534:15–24.

Oldham KB, Spannier J (2006) The Fractional Calculus: Theory and Application of Differentiation and Integration to Arbitrary Order Mineola NY: Dover.

Olson ES (2001) Intracochlear pressure measurements related to cochlear tuning. J Acoust Soc Am 110:349–367.

Oman CM, Marcus EN, Curthoys IS (1987) The influence of semicircular canal morphology on endolymph flow dynamics. An anatomically descriptive mathematical model. Acta Otolaryngol (Stockh) 103:1–13.

Oman CM, Young LR (1972) The physiological range of pressure difference and cupula deflections in the human semicircular canal. Acta Otolaryngol (Stockh) 74:324–331.

Paige GD (1985) Caloric responses after horizontal canal inactivation. Acta Otolaryngol (Stockh) 100:321–327.

Perachio AA, Correia MJ (1983) Responses of semicircular canal and otolith afferents to small angle static head tilts in the gerbil. Brain Res 280:287–298.

Plotnik M, Goldberg JM, Marlinski VV (1999) Excitatory response-intensity relations in afferents from the chinchilla's superior and horizontal canals. Soc Neurosci Abstr 25:663.

Plotnik M, Marlinski V, Goldberg JM (2005) Efferent-mediated fluctuations in vestibular nerve discharge: a novel, positive-feedback mechanism of efferent control. J Assoc Res Otolaryngol 6:311–323.

Pozzo T, Berthoz A, Lefort L (1990) Head stabilization during various locomotor tasks in humans. I. Normal subjects. Exp Brain Res 82:97–106.

Rabbitt RD (1999) Directional coding of three-dimensional movements by the vestibular semicircular canals.[erratum appears in Biol Cybern 2000 Apr;82(4):355]. Biol Cybern 80:417–431.

Au:- Please provide the page numbers for this reference.

Rabbitt RD, Damiano ER, Grant JW (2004a) Biomechanics of the semicircular canals and otolith organs. In: The Vestibular System (Highstein SM, Popper A, Fay RR, eds), pp. 153–201. New York: Springer-Verlag.

Ramachandran R, Lisberger SG (2005) Normal performance and expression of learning in the vestibulo-ocular reflex (VOR) at high frequencies. J Neurophysiol 93:2028–2038.

Ramachandran R, Lisberger SG (2006) Transformation of vestibular signals into motor commands in the vestibuloocular reflex pathways of monkeys. J Neurophysiol 96:1061–1074.

Ramprashad F, Landolt JP, Money KE, Laufer J (1984) Dimensional analysis and dynamic response characterization of mammalian peripheral vestibular structures. Am J Anat 169:295–313.

Reisine H, Simpson JI, Henn V (1988) A geometric analysis of semicircular canals and induced activity in their peripheral afferents in the rhesus monkey. Ann N Y Acad Sci 545:10–20.

Rieke F, Warland D, de Ruyter van Steveninck R, Bialek WS (1997) Spikes. Exploring the Neural Code. Cambridge, MA: MIT Press.

Robles L, Ruggero MA (2001) Mechanics of the mammalian cochlea. Physiol Rev 81:1305–1352.

Ross MD, Komorowski TE, Donovan KM, Pote KG (1987) The suprastructure of the saccular macula. Acta Otolaryngol (Stockh) 103:56–63.

Ross MD, Pote KG (1984) Some properties of otoconia. Philosophical Trans Royal Soc London B Biol Sci 304:445–452.

Rushton WAH (1951) A theory of the effects of fibre size in medullated nerve. J Physiol (Lond) 115:101–122.

Sadeghi SG, Chacron MJ, Taylor MC, Cullen KE (2007a) Neural variability, detection thresholds, and information transmission in the vestibular system. J Neurosci 27:771–781.

Sadeghi SG, Minor LB, Cullen KE (2007b) Response of vestibular-nerve afferents to active and passive rotations under normal conditions and after unilateral labyrinthectomy. J Neurophysiol 97:1503–1514.

Scherer H, Brandt U, Clarke AH, Merbold U, Parker R (1986) European vestibular experiments on the Spacelab-1 mission: 3. Caloric nystagmus in microgravity. Exp Brain Res 64:255–263.

Scherer H, Clarke AH (1985) The caloric vestibular reaction in space. Physiological considerations. Acta Otolaryngol 100:328–336.

Schneider LW, Anderson DJ (1976) Transfer characteristics of first- and second-order lateral canal vestibular neurons in gerbil. Brain Res 112:61–76.

Shannon CE, Weaver W (1949) The Mathematical Theory of Communication. Urbana, IL: University of Illinois Press.

Smith CE, Goldberg JM (1986) A stochastic afterhyperpolarization model of repetitive activity in vestibular afferents. Biol Cybern 54:41–51.

Somps CJ, Schor RH, Tomko DL (1994) Vestibular afferent responses to linear accelerations in the alert squirrel monkey. In: NASA Technical Memorandum 4581. Moffett Field, CA: Ames Research Center.

Spassova MA, Avissar M, Furman AC, Crumling MA, Saunders JC, Parsons TD (2004) Evidence that rapid vesicle replenishment of the synaptic ribbon mediates recovery from short-term adaptation at the hair cell afferent synapse. J Assoc Res Otolaryngol 5:376–390.

Spoor F (1998) Comparative review of the human bony labyrinth. Yearbook of Physical Anthropology 41:211–251.

Stahl JS (1992) Signal Processing in the Vestibulo-ocular Reflex of the Rabbit (PhD thesis). New York: New York University.

Steinhausen W (1931) Ueber den Nachweis der Bewegung der Cupula in der intakten Bogengansampulle des Labyrinthes bei der natürlichen rotatorischen und calorischen Reizung. Pflugers Arch 228:322–328.

Steinhausen W (1935) Über die durch die Otolithen ausgelösten Kräfte. Pflugers Arch 235:538-544.

Stephan H, Frahm H, Baron G (1981) New and revised data on volumes of brain structures ininsectivores and primates. Folia Primatol (Basel) 35:1–29.

Taglietti V, Rossi ML, Casella C (1977) Adaptive distortions in the generator potential of semicircular canal sensory afferents. 123: 41-57.

Thalmann R, Ignatova E, Kachar B, Ornitz DM, Thalmann I (2001) Development and maintenance of otoconia: biochemical considerations. Ann N Y Acad Sci 942:162–178.

Thorson J, Biederman-Thorson M (1974) Distributed relaxation processes in sensory adaptation. Science 183:161-172.

Tomko DL, Peterka RJ, Schor RH (1981a) Responses to head tilt in cat eight nerve afferents. Exp Brain Res 41:216–221.

Tomko DL, Peterka RJ, Schor RH, O'Leary DP (1981b) Response dynamics of horizontal canal afferents in barbiturate-anesthetized cats. J Neurophysiol 45:376–396.

Trincker D (1962) The transformation of mechanical stimulus into nervous excitation by the labyrinthine receptors. Soc Exp Biol (Great Britain) 16: 289-316.

van Egmond AAJ, Groen, J.J., Jongkees LBW (1949) The mechanics of the semicircular canal. J Physiol 110:1–17.

Vollrath MA, Eatock RA (2003) Time course and extent of mechanotransducer adaptation in mouse utricular hair cells: comparison with frog saccular hair cells. J Neurophysiol 90:2676–2689.

Wersäll J (1956) Studies on the structure and innervation of the sensory epithelium of the cristae ampullaris in the guinea pig. A light and electron microscopic investigation. Acta Otolaryngol Suppl (Stockh) 126:1–85.

Yagi T, Simpson NE, Markham CH (1977) The relationship of conduction velocity to other physiological properties of the cat's horizontal canal neurons. Exp Brain Res 30:587–600.

Yang A, Hullar TE (2007) The relationship of semicircular canal size to vestibular-nerve afferent sensitivity in mammals. J Neurophysiol. 98: 3197–3205.

Young JH, Anderson DJ (1974) Response patterns of primary vestibular neurons to thermal and rotational stimuli. Brain Res 79:199–212.

Zhao X, Yang H, Yamoah EN, Lundberg YW (2007) Gene targeting reveals the role of Oc90 as the essential organizer of the otoconial organic matrix. Dev Biol 304:508–524.